AUTOPHAGY
2023, VOL. 19, NO. 7, 2026–2044
https://doi.org/10.1080/15548627.2023.2167689

Taylor & Francis
Taylor & Francis Group

RESEARCH PAPER

OPEN ACCESS Check for updates

Inhibition of autophagy in microglia and macrophages exacerbates innate immune responses and worsens brain injury outcomes

Nivedita Hegdekar[a], Chinmoy Sarkar[a], Sabrina Bustos[a], Rodney M. Ritzel[a,c], Marie Hanscom[a], Prarthana Ravishankar[a], Deepika Philkana[a], Junfang Wu[a], David J. Loane[a,d], and Marta M. Lipinski [a,b]

[a]Department of Anesthesiology and Shock, Trauma and Anesthesiology Research Center, University of Maryland School of Medicine, Baltimore, MD, USA; [b]Department of Anatomy and Neurobiology, University of Maryland School of Medicine, Baltimore, MD, USA; [c]Department of Neurology, McGovern Medical School, University of Texas, Houston, Tx, USA; [d]School of Biochemistry and Immunology, Trinity College, Dublin, Ireland

ABSTRACT

Excessive and prolonged neuroinflammation following traumatic brain injury (TBI) contributes to long-term tissue damage and poor functional outcomes. However, the mechanisms contributing to exacerbated inflammatory responses after brain injury remain poorly understood. Our previous work showed that macroautophagy/autophagy flux is inhibited in neurons following TBI in mice and contributes to neuronal cell death. In the present study, we demonstrate that autophagy is also inhibited in activated microglia and infiltrating macrophages, and that this potentiates injury-induced neuroinflammatory responses. Macrophage/microglia-specific knockout of the essential autophagy gene *Becn1* led to overall increase in neuroinflammation after TBI. In particular, we observed excessive activation of the innate immune responses, including both the type-I interferon and inflammasome pathways. Defects in microglial and macrophage autophagy following injury were associated with decreased phagocytic clearance of danger/damage-associated molecular patterns (DAMP) responsible for activation of the cellular innate immune responses. Our data also demonstrated a role for precision autophagy in targeting and degradation of innate immune pathways components, such as the NLRP3 inflammasome. Finally, inhibition of microglial/macrophage autophagy led to increased neurodegeneration and worse long-term cognitive outcomes after TBI. Conversely, increasing autophagy by treatment with rapamycin decreased inflammation and improved outcomes in wild-type mice after TBI. Overall, our work demonstrates that inhibition of autophagy in microglia and infiltrating macrophages contributes to excessive neuroinflammation following brain injury and in the long term may prevent resolution of inflammation and tissue regeneration.

Abbreviations: *Becn1*/BECN1, beclin 1, autophagy related; CCI, controlled cortical impact; *Cybb*/CYBB/NOX2: cytochrome b-245, beta polypeptide; DAMP, danger/damage-associated molecular patterns; *Il1b*/IL1B/Il-1β, interleukin 1 beta; LAP, LC3-associated phagocytosis; *Map1lc3b*/MAP1LC3/LC3, microtubule-associated protein 1 light chain 3 beta; *Mefv*/MEFV/TRIM20: Mediterranean fever; *Nos2*/NOS2/iNOS: nitric oxide synthase 2, inducible; *Nlrp3*/NLRP3, NLR family, pyrin domain containing 3; *Sqstm1*/SQSTM1/p62, sequestosome 1; TBI, traumatic brain injury; *Tnf*/TNF/TNF-α, tumor necrosis factor; *Ulk1*/ULK1, unc-51 like kinase 1.

ARTICLE HISTORY
Received 19 July 2022
Revised 8 January 2023
Accepted 9 January 2023

KEYWORDS
Autophagy; innate immunity; macrophage; microglia; neuroinflammation; traumatic brain injury

Introduction

Traumatic brain injury is an acquired form of injury caused by an external physical impact to the head resulting in brain damage [1,2]. TBI is a major cause of death in people of all ages and has many short- and long-term consequences in the survivors, with many living with significant long-term motor, cognitive and/or affective disabilities, and decreased quality of life [3]. Additionally, history of TBI is a leading non-genetic factor predisposing to development of neurodegenerative diseases later in life [4,5].

Despite its prevalence and devastating consequences, there are currently no treatments able to effectively improve recovery after TBI. This is due to the complex nature of brain injury and its poor mechanistic understanding [6]. TBI produces tissue damage and neurological dysfunction through both direct mechanical damage (primary injury) and through subsequent cellular and biochemical alterations (secondary injury) [7]. Components of the secondary injury include both neuronal cell death and neuroinflammation, which interact and further exacerbate each other. TBI neuroinflammation is mediated through several cell types including microglia, the resident brain immune cells, and myeloid cells, including macrophages and other monocytes, infiltrating the brain following injury-induced blood-brain-barrier damage [8]. Recruitment of activated phagocytic cells is a normal response to injury in any tissue, important for clearance of dead cells, cellular debris and danger/damage associated molecular patterns (DAMP). Binding and phagocytosis of DAMP lead to activation of innate immune responses including the inflammasome and the type-I interferon pathways [9]. While in short-term these responses are beneficial and can set the stage for tissue regeneration and recovery [10], extensive or prolonged inflammation is detrimental and contributes to

CONTACT Marta M. Lipinski mlipinski@som.umaryland.edu Department of Anesthesiology and Shock, Trauma and Anesthesiology Research Center, University of Maryland School of Medicine, Baltimore, MD, USA

Supplemental data for this article can be accessed online at https://doi.org/10.1080/15548627.2023.2167689

© 2023 The Author(s). Published by Informa UK Limited, trading as Taylor & Francis Group.
This is an Open Access article distributed under the terms of the Creative Commons Attribution-NonCommercial-NoDerivatives License (http://creativecommons.org/licenses/by-nc-nd/4.0/), which permits non-commercial re-use, distribution, and reproduction in any medium, provided the original work is properly cited, and is not altered, transformed, or built upon in any way.

further neurodegenerative processes and neurological dysfunction [9,11,12]. Clinical and experimental data indicate that after brain injury neuroinflammation fails to resolve and in TBI patients can persist for decades after the initial trauma [12–14]. Several studies have shown that pharmacological agents that decrease neuroinflammation or remove neurotoxic microglia are beneficial for recovery after injury [9,15]. However, the reasons for aberrant inflammatory responses after TBI remain poorly understood.

The autophagy-lysosomal pathway is an essential part of cellular catabolism, mediating removal and recycling of damaged proteins, protein aggregates and organelles [16]. In addition to this established role in protein homeostasis and quality control, recent data implicate autophagy as an important regulator of inflammatory responses. The crosstalk between autophagy and inflammation has been documented in diseases associated with organ and systemic inflammation, such as inflammatory bowel diseases [17], type 2 diabetes, cardiac disorders, and cystic fibrosis [18]. Several autophagy genes are also linked to the development of autoimmune diseases [19]. However, the role of autophagy in inflammatory responses in the brain, including in the context of TBI, remains poorly understood.

In general, high levels of autophagy flux in immune cells are associated with anti-inflammatory, and the inhibition of flux, with pro-inflammatory phenotypes [20]. This is thought to be mediated by several mechanisms, including autophagy-dependent regulation of innate immunity. Autophagy is thought to participate in removal and degradation of extracellular inflammatory agonists including dead cells and DAMP through a non-canonical pathway termed LC3-associated autophagy (LAP), decreasing their ability to activate innate immune pathways [21–24]. Autophagy can also affect intracellular innate immune mediators [25,26] by directly targeting and degrading their components through recently discovered precision autophagy [27,28]. This includes targeting of the activated NLRP3 (nucleotide-binding oligomerization domain, leucine rich repeat and pyrin domain containing 3) inflammasome through interaction between autophagy components such as ULK1 and inflammasome components such as NLRP3, with MEFV/TRIM20 protein as adaptor.

We previously demonstrated that autophagy is inhibited in cortical and hippocampal neurons after TBI in the controlled cortical impact (CCI) mouse model, and that this inhibition contributes to neuronal cell death [29,30]. We also observed accumulation of autophagosomes in activated immune cells, suggesting potential role of autophagy in modulating neuroinflammatory responses after injury. In the present study, we examined the crosstalk between autophagy impairment and inflammation after injury using *in vitro* and *in vivo* models. Our data demonstrate that autophagy flux is inhibited in both activated microglia and infiltrating monocyte/macrophage cell populations, and that this impairment potentiates TBI-induced inflammatory responses. Microglia/macrophage-specific knockout of the autophagy gene *Becn1* in mice resulted in a marked exacerbation of the innate immune responses, including activation of the NLRP3 inflammasome and the type-I IFN (interferon) pathways, indicating the importance of autophagy in suppression of innate-immunity mediated inflammation in the brain. Autophagy impairment was associated with decreased phagocytic clearance of DAMP by microglia following injury. Additionally, autophagy impairment in microglia/macrophages contributed to long-term functional defects and increased neurodegeneration following TBI. Conversely, pharmacological stimulation of autophagy in wild-type mice decreased inflammation and improved functional outcomes after injury. Our work expands understanding of molecular mechanisms mediating neuroinflammation after brain injury and preventing its effective resolution. It also identifies activation of autophagy as a potential therapeutic intervention after injury, able to target both neuronal cell death and neuroinflammation.

Results

Autophagy is inhibited in activated microglia and infiltrating monocytes after TBI

We previously demonstrated that inhibition of autophagy flux within the injured cortex occurs at different time points in different cell types following moderate controlled cortical impact (CCI) TBI in mice [29], with activated AIF1/IBA1-positive immune cells showing peak autophagosome accumulation at 3 days after injury.

The immune cells participating in TBI neuroinflammatory responses include both activated resident microglia and infiltrating monocytes/macrophages [8,31]. To distinguish between these cells, we performed moderate CCI on *Cx3cr1-GFP* mice expressing green fluorescent protein (GFP) from the *Cx3cr1* promoter in both microglia and infiltrating myeloid cells [8,32]. We used immunofluorescence (IF) to co-stain cortical sections with antibodies against ADGRE1/F4/80, which is expressed at a higher level in infiltrating monocytes/macrophages than in microglia, and the autophagy receptor protein SQSTM1/p62, which accumulates in cells with impaired autophagy clearance (Figure 1A-B) [33,34]. Consistent with our previous data [29], accumulation of SQSTM1 in immune cells peaked at 3 days after injury. At that time point 13% of all quantified $CX3CR1^+$ cells were positive for SQSTM1; however, 65% of all quantified $CX3CR1^+$ $ADGRE1^+$ cells were positive for SQSTM1 (Figure 1C-D). Therefore, while SQSTM1 accumulation occurred in both microglia ($ADGRE1^{low}$ $CX3CR1^+$) and infiltrating monocytes ($ADGRE1^{high}$ $CX3CR1^+$) following injury, it was more pronounced within the infiltrating cell population.

Inhibition of autophagy in infiltrating monocytes was confirmed using *Ccr2-RFP* reporter mice expressing RFP from the *Ccr2* promoter specifically in macrophages and monocytes recruited to the sites of inflammation [8]. We observed 90% colocalization between autophagy markers LC3 and SQSTM1 in $CCR2^+$ cells at 3 days after injury, confirming pronounced inhibition of autophagy flux within the infiltrating cells (Figure 1E-F) [34]. To ascertain that inhibition of autophagy was also occurring in microglia, we stained sections from *Cx3cr1-GFP* mice with microglial marker TMEM119 and SQSTM1. SQSTM1 immunofluorescence was observed in both $CX3CR1^+$ $TMEM119^-$ and $CX3CR1^+$ $TMEM119^+$ cells, confirming involvement of both infiltrating monocytes and resident microglia (**Fig. S1A**).

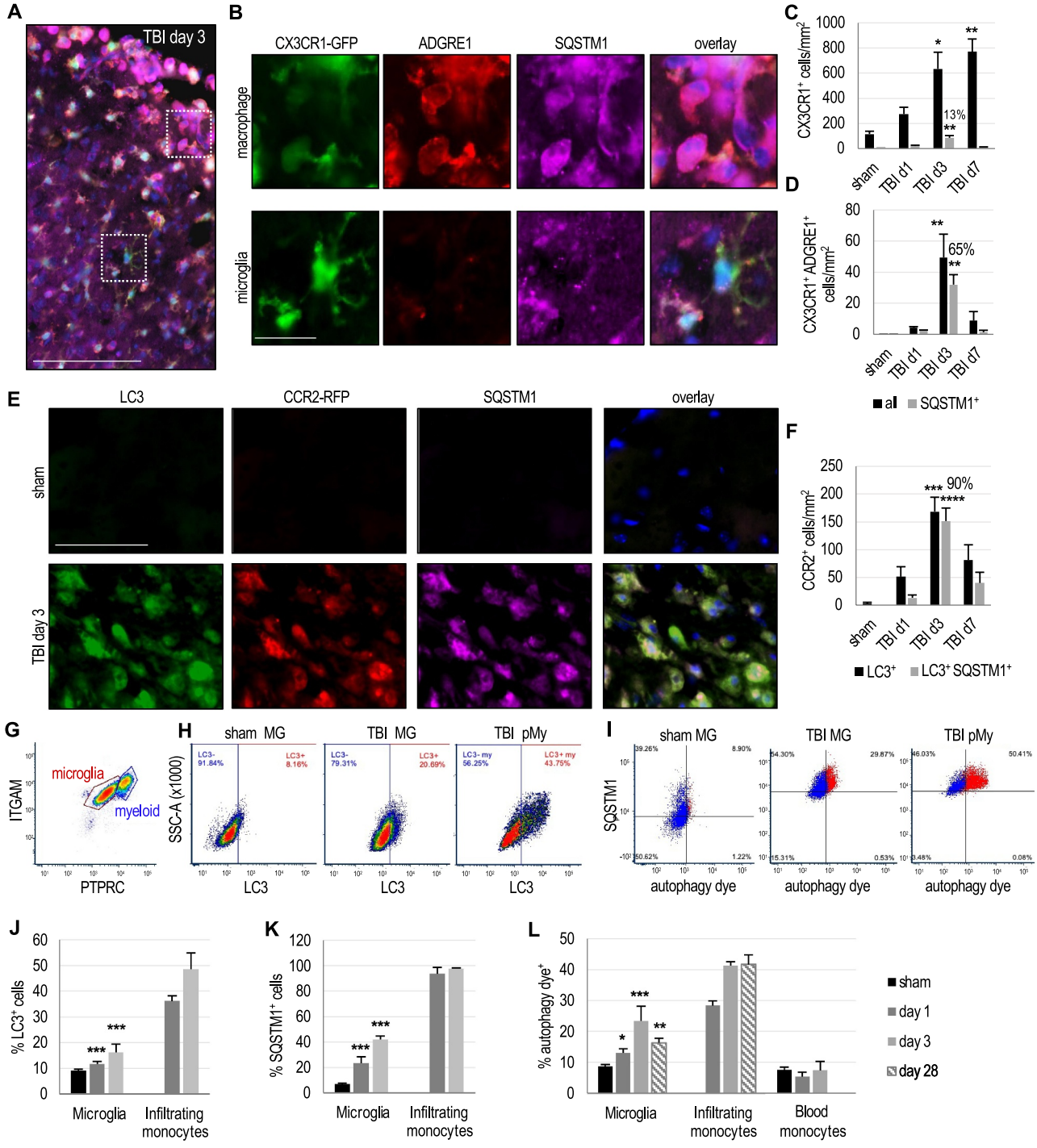

Figure 1. Autophagy is inhibited in activated microglia & macrophages after TBI. (A-B) Images (20X, scale bar: 100 µm) of microglia/macrophage reporter *Cx3cr1-GFP* cortical sections from injured mice (3 days after injury) stained with antibodies against macrophage-specific marker ADGRE1/F4/80 (red) and autophagy flux marker SQSTM1 (purple). White boxes in (A) highlight the cells magnified in (B) (scale bar: 20 µm). Macrophages are defined as CX3CR1^{+}ADGRE1^{high}, and microglia as CX3CR1^{+} ADGRE1^{low}. (C) Corresponding quantification of all CX3CR1^{+} cells (black bars) and CX3CR1^{+} cells with inhibited autophagy (CX3CR1^{+}SQSTM1^{+}, gray bars) in sham, 1-, 3- and 7 days after injury. 13% of all CX3CR1^{+} cells show inhibition of autophagy at 3 days after injury. (D) Quantification of all macrophages (CX3CR1^{+} ADGRE1^{high}, black bars) and macrophages with inhibited autophagy (CX3CR1^{+} ADGRE1^{high} SQSTM1^{+}, gray bars). 65% of all CX3CR1^{+} ADGRE1^{high} cells show inhibition of autophagy at 3 days after injury. Data are mean ± SEM, n = 5 mice/group; *p < 0.05, **p < 0.01 vs. corresponding sham (one-way ANOVA with Dunnet's post-hoc for multiple comparisons). (E) Images (20X, scale bar: 50 µm) of sham and TBI macrophage reporter *Ccr2-RFP* mice cortical sections stained with antibodies against autophagy markers LC3 (green) and SQSTM1 (purple). (F) Corresponding quantification of macrophages (CCR2^{+}) expressing LC3 (black bars) and LC3 plus SQSTM1 (gray bars). 90% of all CCR2^{+} LC3^{+} cells are SQSTM1^{+} at 3 days post TBI. Data are mean ± SEM, n = 4 mice/group; ***p < 0.001, ****p < 0.0001 vs. corresponding sham (one-way ANOVA with Dunnet's post-hoc for multiple comparisons). (G-L) Flow cytometry-based assessment of autophagy in microglia and infiltrating monocytes from sham and TBI mouse cortices. (G) Representative dot plot demonstrating strategy for identification of microglia (PTPRC/CD45^{int} ITGAM/CD11B^{+}) and infiltrating myeloid (PTPRC^{high} ITGAM^{+}) populations at 3 days post TBI. (H) Dot plots demonstrating strategy for identifying cells with normal autophagy (LC3^{-}) and with inhibited autophagy (LC3^{+}) in microglia (MG) and infiltrating myeloid (pMy) cells based on LC3 antibody staining intensity. (I) Comparison of LC3 staining (blue = LC3^{-}, red = LC3^{+}) with Cyto-ID® autophagy dye and SQSTM1 antibody staining. Cells positive for LC3 and autophagy dye also accumulate higher levels of SQSTM1 indicating inhibition of autophagy flux. (J-L) Quantification of microglia and infiltrating macrophages with inhibited autophagy in sham and TBI mouse cortices based on (J) % of LC3^{+} cells, (K) % of SQSTM1^{+} cells, and (L) % of autophagy dye^{+} cells. Analysis of corresponding blood monocytes is included in (L). Data are mean ± SEM; n = 6–7 mice/group; *p < 0.05, **p < 0.01, ***p < 0.001 vs sham; two-way ANOVA with Dunnet's post-hoc for multiple comparisons.

We used flow cytometry as a complementary technique to assess autophagy dynamics in resident microglia (PTPRC/CD45^{int} ITGAM/CD11B^{+}) and infiltrating myeloid cells (PTPRC^{high} ITGAM^{+}, mainly LY6C^{+} monocytes and neutrophils) after TBI (Figure 1G; **Fig. S1B-C**). To assess levels of autophagy we used antibodies against LC3 and SQSTM1, and Cyto-ID® pH-sensitive autophagy dye that fluorescently labels autophagosomes in lysosomally inhibited live cells [35]. All markers showed colocalization, confirming that the same cells accumulated autophagosomes and SQSTM1, consistent with inhibition of autophagy flux (Figure 1H-I). We observed an increase in the number of LC3^{+}, SQSTM1^{+} and autophagy dye^{+} microglia and infiltrating myeloid cells after injury, with levels peaking at 3 days after injury (Figure 1J-L). Consistent with our IF data, all markers accumulated to a higher extent in infiltrating monocytes as compared to resident microglia, indicating higher degree of autophagy inhibition in these cells.

Although overall numbers of activated microglia and especially infiltrating myeloid cells present in the brain decreased after initial peak (**Fig. S1D-E**), a significant number of the remaining cells showed signs of persistent inhibition of autophagy, as indicated by accumulation of autophagy dye up to 28 days after injury (Figure 1L). The percentage of autophagy dye^{+} circulating blood monocytes remains unchanged after injury. This suggests that autophagy impairment within the monocytes is restricted to those that cross the impaired blood-brain barrier and enter brain parenchyma following TBI. Consistent with inhibition of autophagy being unique to the brain, we did not observe accumulation of either LC3-II or SQSTM1 in microglial cells treated with LPS to induce pro-inflammatory polarization *in vitro* (**Fig. S1F-G**).

Inhibition of autophagy is associated with increased expression of pro-inflammatory markers

To determine the inflammatory status of activated microglia and infiltrating monocytes/macrophages with inhibited autophagy flux, we performed IF co-staining using antibodies against SQSTM1 and several inflammatory markers on *Cx3Cr1-GFP* mouse cortical brain sections at 1-, 3-, and 7 days after TBI [29,30]. Consistently with previously published data, we observed significant accumulation of pro-inflammatory markers NOS2/iNOS (nitric oxide synthase 2, inducible), NLRP3 and CYBB/NOX2 (cytochrome b-245, beta polypeptide) in CX3CR1^{+} cells in the injured cortex, with peak at 3 days after injury (Figure 2A-D; **Fig. S2A-C**) [31]. Most of the pro-inflammatory microglia and macrophages also accumulated high levels of SQSTM1, indicating inhibition of autophagy flux in these cells. At 3 days after injury, 69% of the CX3CR1^{+} NOS2^{+} cells, 90% of the CX3CR1^{+} NLRP3^{+} cells, and 89% of the CX3CR1^{+} CYBB^{+} cells were positive for SQSTM1. These findings indicate that inflammatory polarization in microglia and infiltrating monocytes/macrophages is associated with inhibition of autophagy flux.

We used flow cytometry to quantify inflammation in microglia and infiltrating myeloid cells with high versus low levels of autophagy flux. We used Cyto-ID® autophagy dye which reflects autophagosome accumulation, to identify cells with high/normal levels of autophagy flux (dye^{-}), and cells with low levels of autophagy flux/inhibited autophagy flux (dye^{+}), then evaluated levels of pro-inflammatory cytokines in these cell populations in sham and TBI mice. Starting at 1 day after injury, dye^{+} microglia expressed higher levels of pro-inflammatory cytokines, TNF/TNF-α and IL1B/IL-1β, compared to dye^{-} microglia at the same time points (Figure 2E-G). Higher expression of IL1B in dye^{+} microglia compared to dye^{-} microglia persisted up to 28 days after injury, while the higher levels of TNF in the dye^{+} microglia compared to the dye^{-} microglia remained statistically higher at the acute time points but lost significance by day 28 after injury ($p = 0.062$ compared to dye^{-} microglia at day 28). Within infiltrating myeloid cells, we also observed higher levels of both TNF and IL1B levels in the dye^{+} cells after injury (Figure 2H-J), however, this was not statistically significant until the later time points (7 and 28 days after injury). These findings confirm that inhibition of autophagy in microglia and infiltrating myeloid cells is associated with higher levels of pro-inflammatory cytokine production.

Inhibition of autophagy exacerbates inflammatory responses in vitro

Our *in vivo* findings demonstrated that inhibition of autophagy in microglia and monocytes/macrophages after injury is associated with pro-inflammatory phenotypes. To determine if inhibition of autophagy may contribute to the exacerbated neuroinflammation, we performed *in vitro* studies using murine microglia (IMG cells) and murine macrophages (RAW 246.7 cells). We treated cells with inhibitors targeting different stages of autophagy: Bafilomycin A_1 (BafA) to inhibit lysosomal acidification and autophagosome-lysosome fusion; 3-MA to inhibit the class III phosphatidylinositol 3-kinase activity necessary for autophagosome formation; MRT68921 to inhibit ULK1 and autophagy initiation [34,36]. Both IMG and RAW cells treated with autophagy inhibitors had increased inflammation as assessed by elevated levels of NOS2 and NLRP3 proteins and increased nitric oxide production (Figure 3A-F). This was true under baseline conditions, as well as in cells activated by pre-treatment with lipopolysaccharide (LPS). LPS treatment did not affect autophagy flux (Figure 3G). The fact that all three autophagy inhibitors increased levels of the pro-inflammatory markers, suggests that modulation of autophagy (rather than of only one specific component of the pathway) in macrophages and microglia can directly alter inflammatory responses *in vitro*. We observed similar results in primary murine bone marrow derived macrophages (Figure 3H).

Inhibition of autophagy in microglia and infiltrating monocytes exacerbates inflammatory responses after TBI

Lyz2/LysM-cre mice expressing Cre recombinase from the *Lyz2* (lysozyme 2) promoter have been widely used to dissect gene function in macrophages and neutrophils [37]. However, the use of *Lyz2-cre* mice to target genes in microglia is less established. We examined the utility of *Lyz2-cre* in microglia using *ROSA26-lox-STOP-lox-tdTomato* (*ROSA-tdTomato*) reporter mice, which express fluorescent protein, tdTomato,

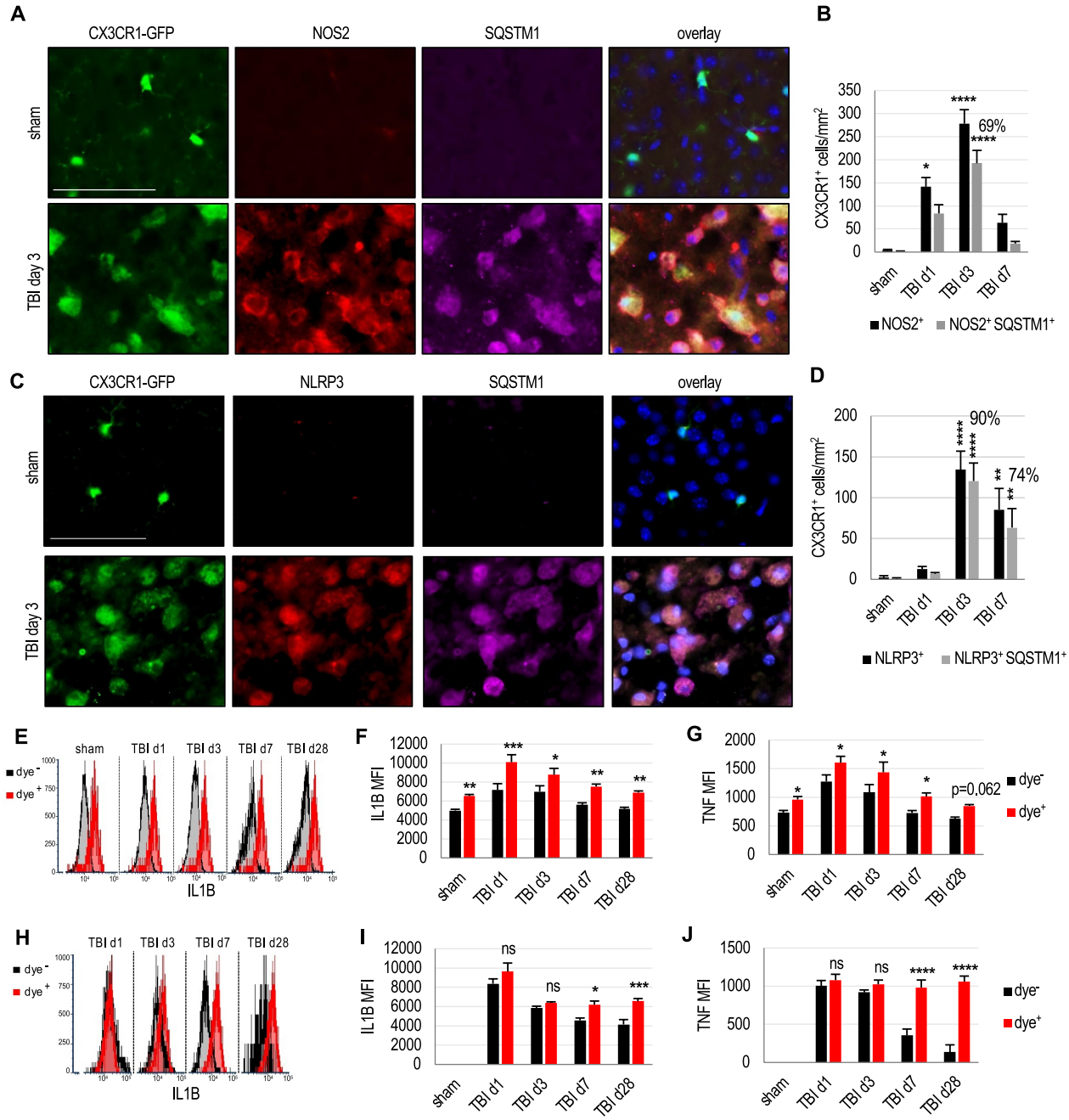

Figure 2. Inhibition of autophagy is associated with increased expression of pro-inflammatory markers after TBI. (A) Images (20X, scale bar: 50 µm) of *Cx3cr1-GFP* cortical sections stained with antibodies against pro-inflammatory cytokine NOS2 (red) and autophagy flux marker SQSTM1(purple). (B) Quantification of IF data from (A) measuring NOS2 expression in all CX3CR1$^+$ cells (black bars) and CX3CR1$^+$ cells with inhibited autophagy (gray bars) in sham, and 1-, 3- and 7 days post TBI cortical sections. 69% of all CX3CR1$^+$ NOS2$^+$ cells show inhibition of autophagy at 3 days post injury. (C) Images (20X, scale bar: 50 µm) of *Cx3cr1-GFP* mouse cortical sections stained with antibodies against inflammasome marker NLRP3 (red) and autophagy flux marker SQSTM1(purple). (D) Quantification of IF data from (C) measuring NLRP3 expression in all CX3CR1$^+$ cells (black bars) and CX3CR1$^+$ cells with inhibited autophagy (gray bars) in sham and 1-, 3- and 7 days post TBI brain cortical sections. 90% of all CX3CR1$^+$ NLRP3$^+$ cells show inhibition of autophagy at 3 days post injury. Data are mean ± SEM, n = 5 mice/group; *p < 0.05, **p < 0.01 vs. corresponding sham (one-way ANOVA with Dunnet's post-hoc for multiple comparisons). (E-J) Flow cytometry-based assessment of inflammatory markers in microglia and infiltrating myeloid cells with normal autophagy flux (Cyto-ID® autophagy dye$^-$, black) versus inhibited autophagy flux (dye$^+$, red) isolated form sham and injured mouse brains at 1-, 3-, 7- and 28- days post TBI. (E) Representative histograms showing comparison of IL1B/IL-1β staining intensity in microglia with normal autophagy flux (black, dye$^+$) and inhibited autophagy flux (red, dye$^-$). (F-G) Quantification of IL1B (F) and TNF/TNF-α (G) MFI in microglia demonstrates increased pro-inflammatory expression levels in cells with inhibited autophagy up to day 28 post injury. (H) Representative histograms showing comparison of IL1B staining intensity in infiltrating myeloid cells with normal (black) and inhibited autophagy flux. (I-J) Quantification of IL1B (I) and TNF (J) mean fluorescence intensity (MFI) in infiltrating myeloid cells. Data are mean ± SEM, n = 6–7 mice/group; *p < 0.05, **p < 0.01, ***p < 0.001, ****p < 0.0001 vs. corresponding autophagy dye$^-$ group; two-way ANOVA with Bonferroni's post-hoc for multiple comparisons.

only following cre-mediated recombination [38]. Our flow cytometry data demonstrated that approximately half of the microglia (PTPRC^{int} ITGAM$^+$) isolated from both sham and TBI *Lyz2-cre/ROSA-tdTomato* mouse brains expressed tdTomato, indicating Cre mediated recombination. As expected, in TBI mice, over 80% of infiltrating monocytes (PTPRC^{high} ITGAM$^+$) were tdTomato$^+$ (Figure 4A; **Fig. S3A**). Thus, *Lyz2-cre* is active in approximately half of

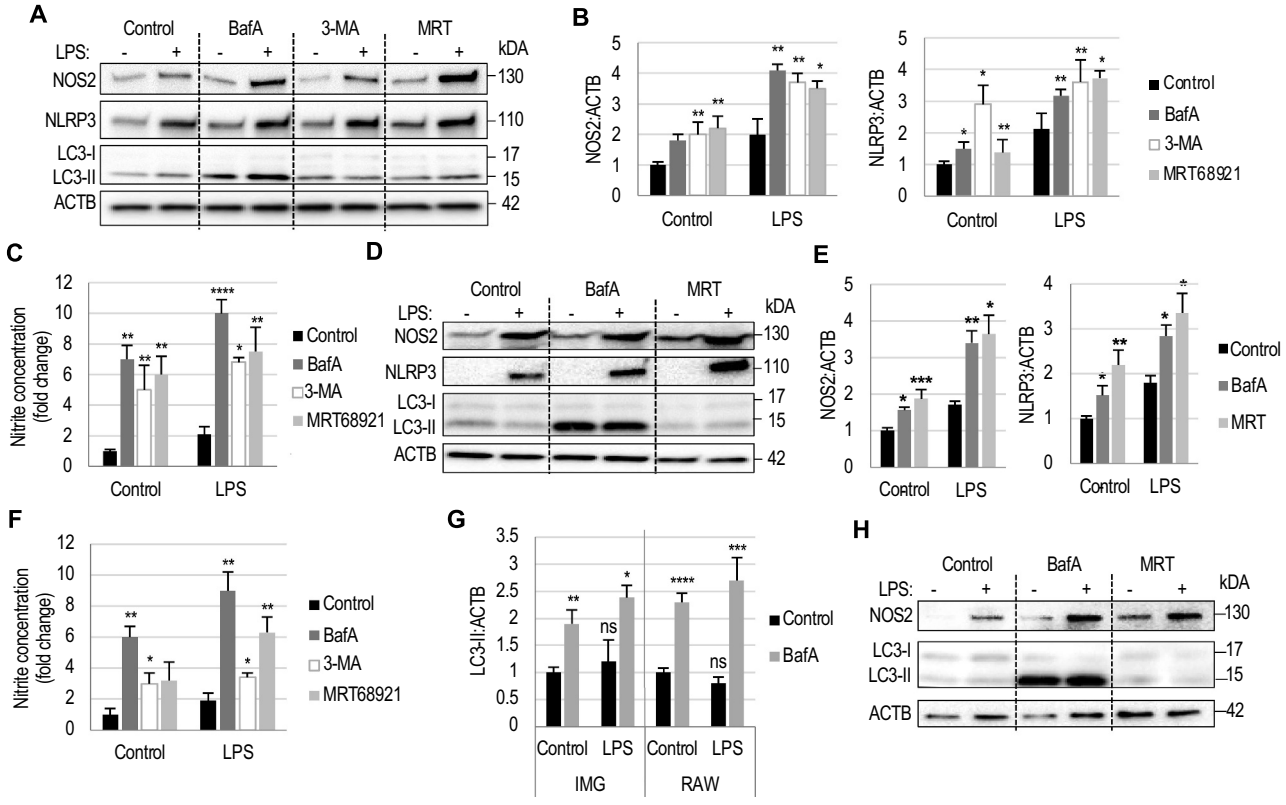

Figure 3. Inhibition of autophagy in macrophages and microglia exacerbates inflammatory responses *in vitro*. (A) Western blot of murine IMG microglial cells treated with autophagy inhibitors bafilomycin A_1 (BafA, 20 nM), 3-methyladenine (3-MA, 100 μM), or MRT68921 (MRT, 10 μM) for 6 h with or without lipopolysaccharide (LPS) pre-treatment (10 ng/μl, 3 h). (B) Densitometric analysis from (A) demonstrating increased NOS2 and NLRP3 protein expression (proteins normalized to loading control ACTB/β-Actin) in IMG microglial cells treated with autophagy inhibitors, under both basal conditions and following LPS pre-treatment. (C) Griess assay demonstrating increased nitric oxide production in IMG microglial cells treated with autophagy inhibitors as described in (A). (D) Western blot of murine RAW 246.7 macrophage cells treated with autophagy inhibitors as described in (A). (E) Densitometric analysis from (D) demonstrating increased NOS2 and NLRP3 protein expression in RAW cells treated with autophagy inhibitors, under both basal conditions and following LPS pre-treatment. (F) Griess assay demonstrating increased nitric oxide production in RAW macrophage cells treated with autophagy inhibitors as described in (A). (G) Densitometric analysis of LC3-II and SQSTM1 protein levels from (A) and (D) indicating that inflammation (LPS treatment) itself does not lead to inhibition of autophagy flux in IMG and RAW cells. (H) Western blot of *C57Bl/6* bone marrow derived macrophages (BMDM) showing increased expression of NOS2 protein levels when treated with autophagy inhibitors as described in (A). Data are mean ± SEM; n = 3 replicates/group with 3 independent experiments performed. *p < 0.05, **p < 0.01, ***p < 0.001, ****p < 0.0001, vs corresponding control; one-way ANOVA with Tukey's post-hoc for multiple comparisons.

microglia and majority of infiltrating monocytes, making it a useful driver to study the role of microglia and macrophages in neuroinflammation after brain injury.

To assess the role of microglial and macrophage autophagy in inflammation after TBI, we crossed *Lyz2-cre* and conditional autophagy deficient *Becn1*$^{flox/flox}$ mice [39]. Homozygous *Lyz2-cre/Becn1-flox* (*becn1 cKO*) mice had decreased *becn1* mRNA levels in the brain as well as in isolated BMDMs as compared to *Lyz2*$^{Cre/Cre}$ controls (**Fig. S3B-C**). In BMDMs decrease in BECN1 protein was confirmed by western blot **(Fig. S3D).**

To determine the neuroinflammatory consequences of autophagy inhibition in microglia and infiltrating macrophages, we evaluated gene expression in sham and TBI (3 days after TBI) cortex from *Lyz2-cre* (control) and *becn1 cKO* mice using NanoString Neuroinflammation panel including 757 genes within three themes: Immunity & Inflammation, Neurobiology & Neuropathology, and Metabolism & Stress (**Table S1**) [35]. Partial Least-Squares Discriminant Analysis (PLS-DA) of all normalized gene counts revealed clustering of the four experimental mouse groups (control sham, *becn1 cKO* sham, control TBI, *becn1 cKO* TBI) across the first two principal coordinates, which accounted for 75.2% (injury effect) and 4.5% (genotype effect), respectively, of the total variation across samples (Figure 4B). Inter-group differences were confirmed by Euclidean distancing and ward clustering analyses, which segregated the mice into four groups based on injury and genotype (Figure 4C). Based on the clustering patterns, we observed slight overlap between the control sham and *becn1 cKO* sham groups; the control TBI and *becn1 cKO* TBI groups showed better separation. This suggests that inhibition of autophagy in microglia and macrophages in *becn1 cKO* mice, leads to neuroinflammation-related transcriptional changes and that these changes are exacerbated following TBI.

Both genotype- and injury-induced transcriptional differences were confirmed in pairwise comparisons between groups. (Figure 4D; **Fig. S4A**). As expected, significant changes in inflammatory gene expression were observed between sham and TBI groups of both *becn1 cKO* and control mice (**Fig. S4A**). There was a strong overlap between genes differentially expressed in TBI versus sham groups of both control and *becn1 cKO* mice, with 263 out of 333 and 379, respectively, genes in common, consistent with strong pro-inflammatory injury effect irrespective of genotype (**Fig. S4B-C**).

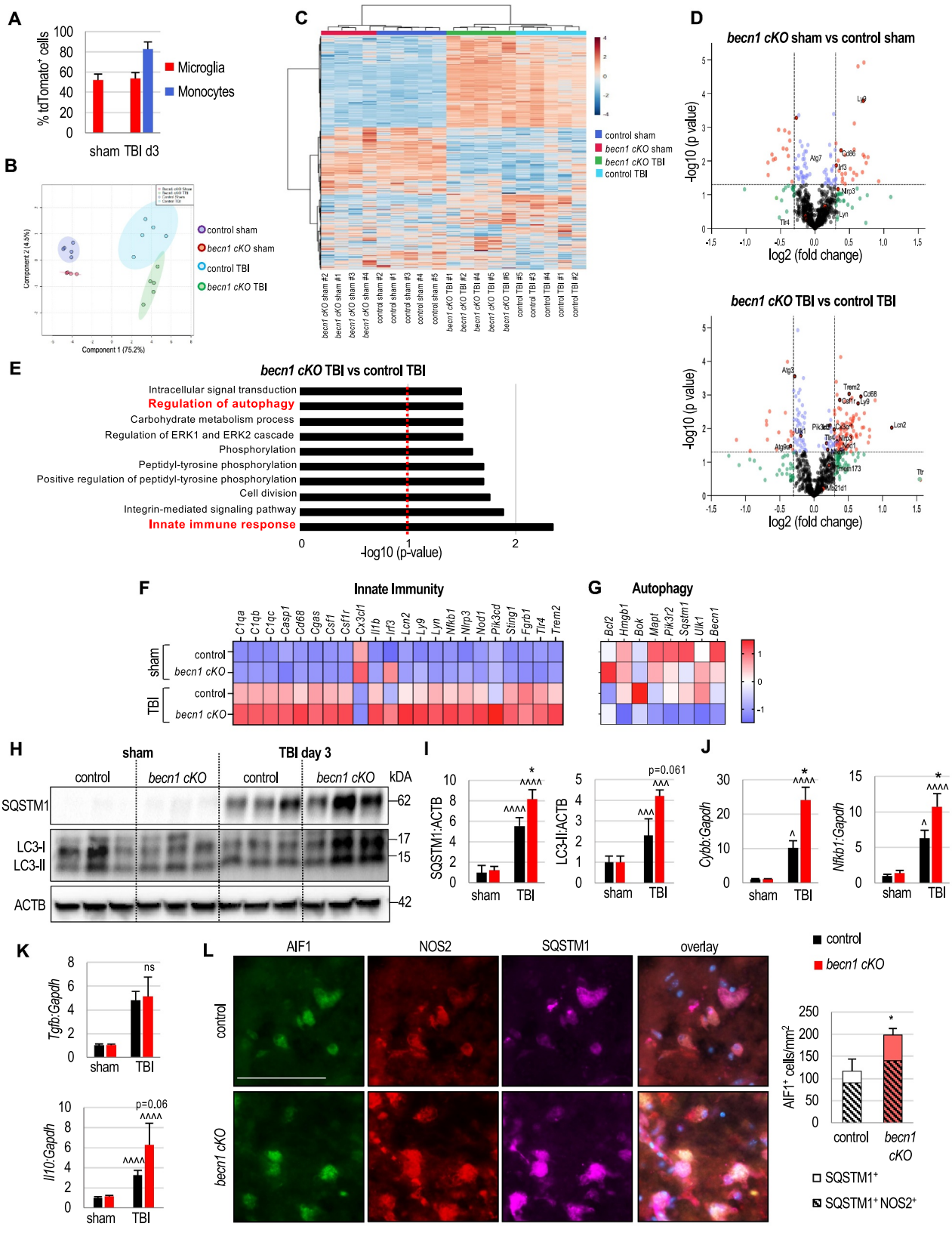

Figure 4. Microglia and monocyte-specific inhibition of autophagy exacerbates inflammatory responses after TBI. (A) Quantification of microglia and infiltrating monocytes that are tdTomato^{+}, indicative of Lyz2-Cre expression. (B-G) Results of NanoString analysis comparing neuroinflammatory gene expression in cortical tissue from sham and TBI (3 days post injury) control (*Lyz2-cre*) mice and mice with microglia and macrophage-specific inhibition of autophagy (*Lyz2-cre/Becn1-flox*, abbreviated as *becn1 cKO*). (B) Partial Least Squares – Discriminate Analysis (PLS-DA) plot demonstrating separation among control sham (purple), *becn1 cKO* sham, control TBI (blue), and *becn1 cKO* TBI (green) mice groups; R2 = 0.98, Q2 = 0.81. Each point represents a data set from an individual animal. The 95% confidence intervals are indicated by elliptical shaded areas. Data were sum normalized, log transformed, and mean centered. (C) Heatmap including all assessed genes based on t-test/ANOVA, Euclidean distancing, and ward clustering. (B-C) were generated using MetaboAnalyst. (D) Volcano plot highlighting differentially expressed genes between *becn1 cKO* and control mice in sham (top) and TBI (bottom) cortices. Genes with $p < 0.05$ and fold change > 2 are highlighted in red. (E) Pathways analysis

Pairwise comparison between control sham versus *becn1 cKO* sham, and control TBI versus *becn1 cKO* TBI revealed significant genotype dependent differences between both sham and TBI groups, with 100 and 175 differentially expressed genes, respectively (Figure 4D**; Fig. S4D**). Only 30 of these genes overlapped (**Fig. S4D**). Pathway analysis of genes differentially expressed between *becn1 cKO* TBI and control TBI mice revealed "innate immune response" as the most highly enriched pathway (Figure 4E). Importantly, "regulation of autophagy" was also included as one of the top differentially expressed pathways. Analysis of individual gene NanoString data confirmed upregulation of genes related to innate immunity and downregulation of autophagy regulating genes in *becn1 cKO* TBI versus control TBI brains (Figure 4F-G**; Fig S4E**). While differences between *becn1 cKO* sham and control/sham mice were not as pronounced as those between *becn1 cKO* TBI and control TBI mice, functional clustering analyses revealed enrichment of several pathways, including those related to immunity and immune responses (**Fig. S4F-G**). This is consistent with our *in vitro* data indicating exacerbated inflammatory responses upon inhibition of autophagy under both baseline and pro-inflammatory (LPS) conditions.

We confirmed NanoString data at the RNA and protein levels. Consistent with decreased *Becn1* gene expression in both sham and TBI *becn1 cKO* mice (**Fig S3B**), we observed exacerbated inhibition of autophagy flux, as demonstrated by increased accumulation of LC3-II and SQSTM1 proteins in the *becn1 cKO* TBI brains as compared to control TBI at 3 days post TBI (Figure 4H-I). Levels of *Sqstm1* or *Map1lc3* mRNA were either not changed or slightly decreased, consistent with regulation at the protein level (**Fig. S4H**). Our analysis also confirmed upregulation of pro-inflammatory genes such as *Cybb* and *Nfkb1* while anti-inflammatory genes such as *Tgfb* and *Il10* were not consistently changed in *becn1 cKO* TBI as compared to control TBI (Figure 4J-K). Immunofluorescence staining confirmed inhibition of autophagy and increased neuroinflammation in *becn1 cKO* mice after injury. At 3 days after injury, we observed greater accumulation of SQSTM1 and pro-inflammatory markers NOS2 in AIF1-positive immune cells in the injured cortex. (Figure 4L).

Inhibition of precision autophagy exacerbates innate immune responses after TBI

Our NanoString pathway analysis implicated innate immune responses as mediators of excessive TBI neuroinflammation in *becn1 cKO* as compared to control mice. This included exacerbation of both the inflammasome and the type I IFN pathway. We confirmed involvement of both pathways using qRT-PCR, which revealed increased mRNA levels of the type I IFN pathway genes *Sting1, Cgas* and *Ifnb1* as well as the inflammasome pathway genes *Nlrp3, Casp1* and *Il1b* in *becn1 cKO* TBI as compared to control TBI mice (Figure 5A-B). These findings were confirmed at the protein level, where we observed increased levels of pro-inflammatory CYBB, CGAS, STING1 and NLRP3 proteins in *becn1 cKO* as compared to control mice at 3 days after injury (Figure 5C-D). Flow cytometry analysis further confirmed exacerbated activation of inflammasomes, as indicated by increased levels of IL1B in both microglia and infiltrating monocytes in *becn1 cKO* as compared to control mice after injury (Figure 5E-H). Increased expression of IL1B was not due to differences in total numbers of activated microglia or infiltrating myeloid cells between control and *becn1 cKO* mice (**Fig. S5A**). Consistent with a specific role of innate immune pathways in autophagy-deficient microglia and monocytes, no significant changes were observed in levels of TNF (**Fig. S5B-E**).

Components of the innate immune pathways can be directly targeted for autophagic degradation via precision autophagy [28,40]. Rather than the general autophagy receptors such as SQSTM1, precision autophagy relies on members of the tripartite motif (TRIM) family to target specific cytoplasmic regulators of innate immunity. MEFV/TRIM20 has been shown to target inflammasome components, including NLRP3, NLRP1, and proCASP1 (caspase 1), for autophagic degradation. MEFV also serves as a platform for the assembly of ULK1, BECN1, and ATG16L1 complexes. This suggests that MEFV acts as an autophagy receptor for delivery of inflammasome components for autophagic degradation [27]. In addition to NLRP3, we observed increased accumulation of MEFV protein in the cortex of *becn1 cKO* TBI as compared to control TBI mice (Figure 5I-J). Levels of *Mefv* mRNA remained unchanged (Figure 5K). This is similar to situation observed for SQSTM1 (Figure 4H-J) and suggests regulation at the protein degradation level. Supporting inhibition of precision autophagy as a mechanism contributing to exacerbated neuroinflammation, our immunoprecipitation analyses demonstrated increased accumulation of protein complexes containing ULK1, MEFV and NLRP3 in injured as compared to sham cortices (Figure 5L).

using NIH-DAVID indicates that innate immune responses are the most differentially regulated between *becn1 cKO* and control mice in the injured cortex after TBI. (F) Nanostring based heatmap shows increased expression innate immunity genes in the injured cortex of *becn1 cKO* compared to control mice at 3 days post injury. Color coding was based on z-score scaling. (G) Nanostring based heatmap shows decrease in autophagy gene expression in the injured cortices of *becn1 cKO* mice compared to control mice at 3 days post injury. Color coding was based on z-score scaling. (H) Western blot of cortical tissue lysates demonstrating that *becn1 cKO* mice have increased impairments in autophagy compared to control mice after TBI (3 days post injury). (I) Densitometric analysis from (H) shows increased expression of autophagy proteins LC3-II and SQSTM1 in *becn1 cKO* as compared to control mice at 3 days post injury. (J) qRT-PCR demonstrating that pro-inflammatory genes *Cybb* and *Nfkb1* are significantly higher in the injured cortices of *becn1 cKO* mice compared to control mice at 3 days post injury. (K) qRT-PCR demonstrating that anti-inflammatory genes *Il10* and *Tgfb* levels are not significantly changed in the injured cortices of control and *becn1 cKO* mice at 3 days post injury. Data are mean ± SEM; n = 5–6 mice/group. *p < 0.05, **p < 0.01, ***p < 0.001 vs corresponding control; ^^^p < 0.001, ^^^^p < 0.0001 vs corresponding sham (two-way ANOVA with Tukey's post-hoc for multiple comparisons). (L) Images (20X, scale bar: 50 µm) of control and *becn1 cKO* cortical sections at 3 days post TBI, stained with antibodies against immune cell marker AIF1/IBA1 (green), pro-inflammatory marker NOS2 (red), and autophagy flux marker SQSTM1 (purple). Corresponding quantification of microglial/macrophage cells with inhibited autophagy ($AIF1^+$ $SQSTM1^+$) and increased NOS2 expression ($AIF1^+$ $SQSTM1^+$ $NOS2^+$). Data are presented as mean ± SEM; n = 4–5 mice/group. *p < 0.05 vs control ($AIF1^+$ $SQSTM1^+$ cells, Student's t-test).

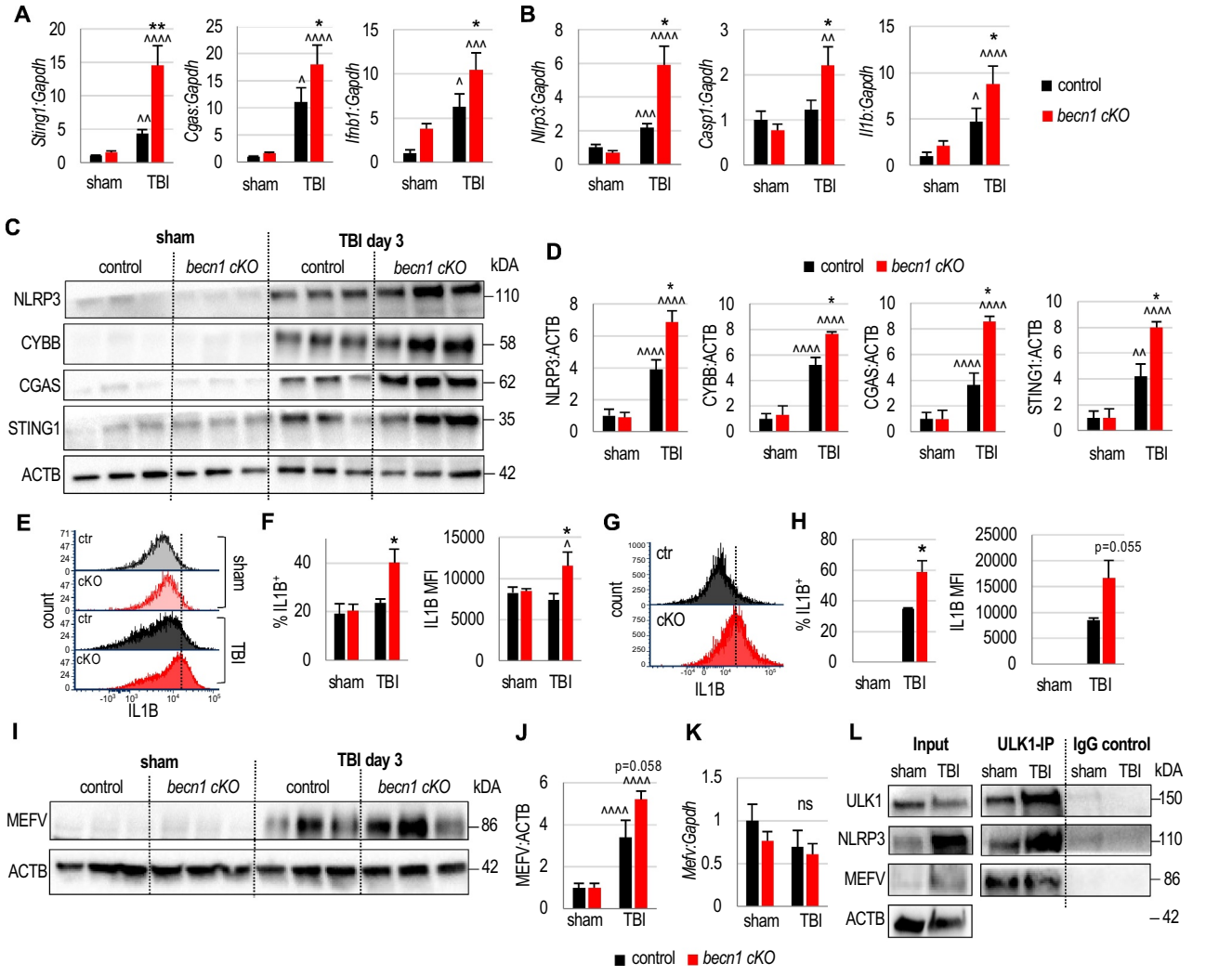

Figure 5. Inhibition of precision autophagy in microglia/monocytes contributes to exacerbated innate immunity responses after TBI. (A-B) qRT-PCR analysis shows increased expression of innate immunity genes related to (A) type-I IFN pathway and the (B) NLRP3 inflammasome pathway in the injured cortices of *becn1 cKO* mice compared to control mice at 3 days post injury. (C) Western blot of cortical tissue lysates demonstrating exacerbated innate immune responses in *becn1 cKO* mice compared to control mice at 3 days post injury. (D) Densitometric analysis from (C) shows increased protein levels of NLRP3, CYBB, CGAS and STING1 in the injured cortical tissue of *becn1 cKO* mice compared to control mice at 3 days post TBI. (E-G) Flow cytometry analysis comparing levels of IL1B protein expression in microglia and infiltrating monocytes from sham and TBI (3 days post injury) cortices of *becn1 cKO* and control mice. (E) Representative histograms comparing relative fluorescence intensity of IL1B in microglia from sham and TBI (3 days post injury) control (ctr) and *becn1* cKO (cKO) cortices. (F) Quantification of IL1B expression and MFI in *becn1 cKO* as compared to control microglia. (G) Representative histogram comparing IL1B expression in infiltrating monocytes from sham and TBI (3 days post injury) control and *becn1* cKO brain cortices. (H) Quantification of % of IL1B$^+$ cells expression and MFI of IL1B in *becn1 cKO* as compared to control infiltrating macrophages. (I) Western blot demonstrating increased accumulation of precision autophagy adaptor protein MEFV in the injured cortex of *becn1 cKO* mice at 3 days post injury. (J) Densitometric analysis of MEFV protein levels with respect to loading control ACTB from (J) . (K) qRT-PCR analysis indicates that *Mefv* mRNA levels do not significantly change in the injured cortex between control and *becn1 cKO* mice. (L) Immunoprecipitation of mouse cortical lysates with antibody against ULK1 but not control IgG leads to co-precipitation of MEFV and NLRP3, demonstrating formation of ULK1-MEFV-NLRP3 complexes at 3 days post injury. Data are mean ± SEM; n = 4–5 mice/group. *p < 0.05, ***p < 0.001, vs. control (genotype effect); ^p < 0.05, ^^p < 0.01, ^^^^p < 0.0001 *vs*. corresponding sham (injury effect); two-way ANOVA with Tukey's post-hoc for multiple comparisons.

Inhibition of autophagy in microglia and infiltrating monocytes leads to defects in phagocytosis and accumulation of DAMPs

Injured cells release DAMPs, which serve as endogenous danger signals that induce phagocytosis of dead cells and cellular debris (efferocytosis) and activate innate immune responses during noninfectious inflammation [22,41]. Using western blotting, we observed higher levels of cleaved SPTAN1/α-FODRIN and PRDX6 in the *becn1 cKO* mice as compared to controls after TBI, suggesting a possible deficiency in DAMP removal (Figure 6A,B). This was likely not caused by defects in cargo recognition as our NanoString data indicated increased rather than decreased expression of scavenger receptors in *becn1 cKO* TBI versus control TBI mice (Figure 6C).

In addition to canonical autophagy, BECN1 is required for non-canonical autophagic pathway termed LC3-associated phagocytosis (LAP), which uses components of the autophagy pathway to mediate efferocytosis and phagocytosis of DAMPs [21]. Using flow cytometry, we measured the ability of microglia and infiltrating monocytes from *becn1 cKO* and control mouse brains to phagocytose fluorescent latex beads. We observed that the phagocytic activity of *becn1* cKO microglia was significantly

reduced as compared to control mice after injury (Figure 6D-F). Phagocytosis differences were also observed in infiltrating monocytes, however, failed to reach significance (**Fig. S5F-G**).

In addition to components of the autophagic machinery, LAP requires recruitment and activity of the NADPH oxidase-2 (CYBB/NOX2) complex to the LC3-associated phagosomes [22]. To determine if LAP may be involved in DAMP clearance after injury, we IF stained sections form sham and day 3 TBI transgenic mice expressing GFP-LC3 autophagy reporter [29]. Confirming potential involvement of LAP, we observed accumulation of both GFP-LC3 and CYBB in activated microglia/macrophages after injury (Figure 6G-H). At higher magnification, some of the GFP-LC3 intracellular puncta were positive for CYBB, identifying them as LAP phagosomes rather than autophagosomes (Figure 6I). These data indicate that similarly to overall autophagy, LAP may be inhibited in activated microglia and macrophages after injury, contributing to impairment in DAMP removal and increased neuroinflammation.

Inhibition of autophagy in microglia and infiltrating monocytes worsens functional recovery after injury

We assessed whether inhibition of autophagy in microglia and monocytes affects motor and memory function in the injured mice [30,42]. We did not observe any differences in motor coordination as assessed by beam walk (**Fig. S6A-B**). We tested spatial learning and memory using Morris Water

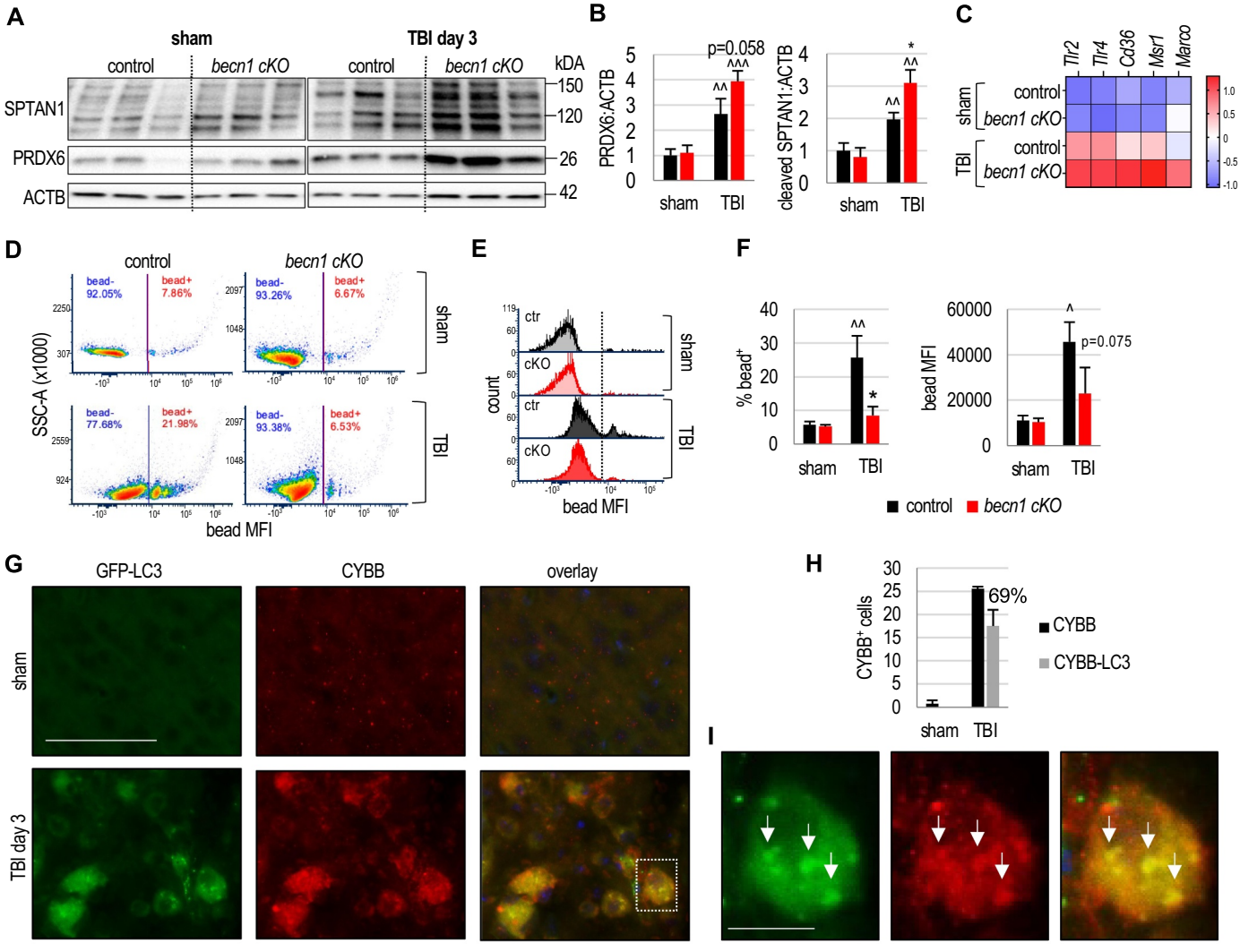

Figure 6. Inhibition of precision autophagy in microglia/monocytes leads to defects in phagocytosis and accumulation of DAMPs after TBI. (A) Western blot of cortical lysates of sham and TBI mice (3 days post injury) comparing levels of DAMP marker PRDX6 and cleaved SPTAN1/α-FODRIN. All lanes are cropped from the same western blot. (B) Densitometric analysis from (A) indicates increase in PRDX6 and cleaved SPTAN1 protein levels in *becn1 cKO* mice compared to control mice at 3 days post injury. (C) NanoString based heatmap of scavenger receptor genes shows increased expression of scavenger receptors in the injured cortices of *becn1 cKO* mice compared to control mice at 3 days post TBI. Color coding was based on z-score scaling. (D) Representative dot plot showing phagocytosis of red beads by control and *becn1 cKO* microglia under sham and TBI (3 days post injury) conditions. (E) Representative histograms comparing relative intensity of phagocytic bead uptake by control mice (black) and *becn1 cKO* microglia (red). (F) Corresponding quantification demonstrates decreased phagocytic bead uptake by *becn1 cKO* microglia compared to control microglia after TBI (3 days post injury). (G) Images (20X, scale bar: 50 μm) of sham and TBI *GFP-Lc3* mice brain cortical sections stained with antibodies against CYBB (red). (H) Quantification of IF data from (G) shows increased colocalization of LC3 and CYBB in cells at 3 days post injury, indicating a potential role of LAP after TBI. (I) Magnification (scale bar: 10 μm) of the white box in (G) highlighting colocalization between LC3 and CYBB. Data are mean ± SEM; n = 4–5 mice/group. *p < 0.05, vs. control (genotype effect); ^p < 0.05, ^^p < 0.01 *vs.* corresponding sham (injury effect); two-way ANOVA with Tukey's post-hoc for multiple comparisons.

Maze (MWM) at 21–25 days after TBI. Consistent with lack of differences in motor function we did not observe genotype-dependent differences in the average swim speed between any of the groups (**Fig. S6C**). During the probe trial, *becn1 cKO* TBI mice spent significantly less time in the escape quadrant as compared to the control TBI group, indicating exacerbated impairment in spatial learning (Figure 6A). We also observed significant differences in the search strategies used during the probe trial. Both *becn1 cKO* sham and control sham mice used either spatial or sequential search strategy. While both TBI groups increasingly relied on a looping strategy to locate the platform, this was more pronounced among the *becn1 cKO* TBI (68.5%) as compared to the control TBI (50%) mice (Figure 7B-C).

To assess non-spatial declarative memory, we performed Novel Object Recognition test at 15–17 days after injury. We did not observe any genotype-dependent differences in distance traveled during the habituation phase (**Fig. S6D**). During the test phase, TBI mice spent less time with the novel object as compared to corresponding sham groups, confirming expected injury effect. However, *becn1 cKO* TBI mice spent significantly less time with the novel object as compared to the control TBI mice (Figure 7D), suggesting that inhibition of autophagy in microglia and monocytes/macrophages exacerbates declarative memory impairments after injury.

To test the effect of autophagy inhibition in microglia and infiltrating monocytes on overall tissue damage and neurodegeneration following TBI, we compared lesion volume and neuronal cell counts in the hippocampus between *becn1 cKO* TBI and control TBI mice at day 28 following injury [43]. While we observed a slight increase in lesion volume in *becn1 cKO* mice as compared to control mice after injury, this failed to reach significance ($p = 0.074$, **Fig. S6E-F**). However, *becn1 cKO* TBI mice had significantly decreased neuronal cell counts in the dentate gyrus (DG) of the ipsilateral hippocampus as compared to control TBI mice, indicating increased neuronal loss (Figure 7E-F). Together, these data suggest that increased inflammation mediated through autophagy inhibition in microglia and infiltrating monocytes exacerbates TBI-induced neurodegeneration. Our qRT-PCR data also indicated that at day 28 after injury, overall innate immunity gene expression remained higher in *becn1 cKO* TBI as compared to control TBI mice, though individual differences did not reach significance (Figure 7G**; Fig. S6G**).

Increasing autophagy reduces neuroinflammation and improves functional outcomes after TBI

Our data indicate that inhibition of autophagy contributes to prolonged neuroinflammation and poor functional recovery after TBI. To determine if increasing autophagy can be used therapeutically to decrease neuroinflammation and improve functional outcomes, we treated wild-type mice with an MTOR inhibitor and a known autophagy inducer, rapamycin. Following treatment with rapamycin, TBI mice showed improved memory, as assessed by performance in MWM and Y-Maze tasks, as compared to vehicle-treated TBI mice (Figure 7H**; Fig S7A**). qRT-PCR analyses at 3 days post injury indicated overall decrease in expression of genes related to innate immunity and inflammation, however individual gene data did not reach significance (Figure 7I**; Fig S7B**). On the other hand, rapamycin treatment resulted in significantly decreased levels of NLRP3, CGAS and STING1 proteins (Figure 7J-K). This is consistent with the ability of increased autophagy to control levels of innate immune mediators via protein degradation. Together, these data provide further evidence of anti-inflammatory effect of increased autophagy following TBI.

Discussion

Acute inflammation is a physiological response to infection, insult or injury that eliminates or neutralizes foreign organisms or any generated tissue and cellular debris. It is generally followed by resolution of inflammation, which prevents excessive injury and promotes restoration of tissue structure and function. The reasons for the excessive levels of neuroinflammation and the failure of inflammation to resolve after brain injury are not clear [13]. In the present study, we explored the role of autophagy in modulating neuroinflammatory responses in mice following TBI. We demonstrate that autophagy is inhibited after TBI in activated microglia and infiltrating macrophages and that this contributes to excessive neuroinflammation. Our data also demonstrate that inhibition of autophagy persists for at least 4 weeks post injury and is associated with increased neuronal loss and worse cognitive outcomes, while increasing autophagy can attenuate neuroinflammation and improve outcomes. Therefore, inhibition of autophagy may be a contributing factor to both excessive inflammatory responses observed following brain injury, as well as to the failure of these responses to resolve over time, resulting in poor TBI outcomes.

Most of our existing knowledge on the autophagy-inflammation link is derived from studies in peripheral macrophages and epidemiological data linking autophagy defects with the development of autoimmune and inflammatory diseases. Generally, inhibition of autophagy flux in peripheral macrophages results in increased pro-inflammatory polarization. For example, loss of the autophagy protein ATG16L1 is associated with Crohn disease and results in enhanced pro-inflammatory cytokine production by macrophages in response to stress [44], whereas a conditional knockout of *Atg5* or *Atg7* in murine macrophages increased severity of uveitis [45] and liver fibrosis [46]. Much less is known what role autophagy may play in the regulation of inflammatory responses in the CNS. In particular, the role of autophagy in neuroinflammation after brain injury has remained controversial, with both pro-inflammatory and anti-inflammatory roles proposed [47,48]. This may be due to the confounding effects of perturbing autophagy at the organismal level rather than in cell type specific manner. Our data demonstrate that inhibition of autophagy in microglia and infiltrating monocytes leads to exacerbated neuroinflammation and activation of the innate immunity pathways after TBI. This is consistent with recently reported neuroinflammation, inflammasome activation and consequent motor deficits, observed in aged mice with a microglia-specific knock out of

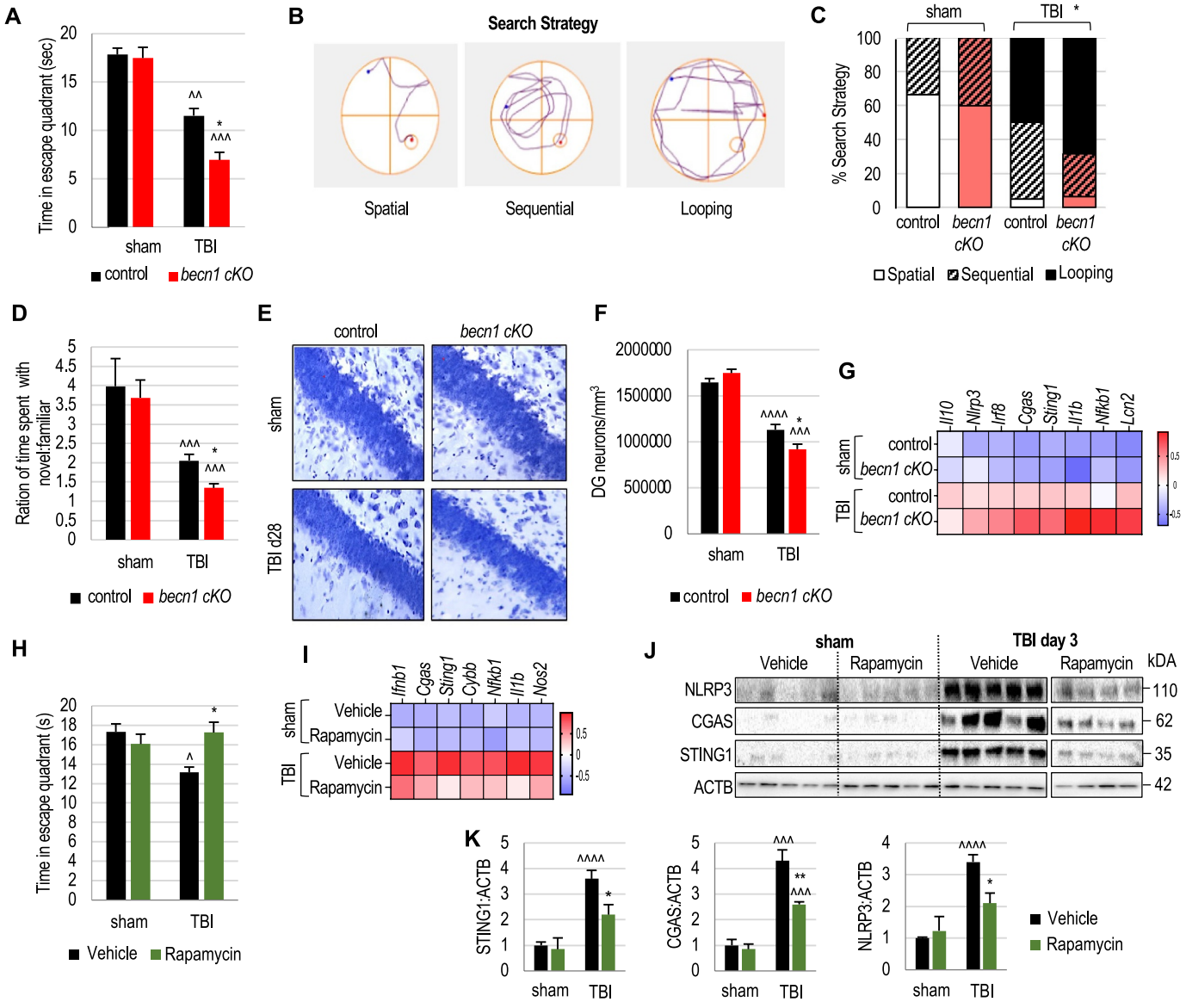

Figure 7. Inhibition of autophagy in microglia/monocytes worsens, while stimulation of autophagy improves long-term cognitive outcomes after TBI. (A-C) Deficits in spatial learning and memory measured using Morris Water Maze (MWM) during days 21–25 following TBI. (A) During the probe trial testing, *becn1 cKO* mice spent significantly less time searching for the escape quadrant compared to control mice after injury. (B) Representative images for search strategy assessment for probe trial testing. (*p < 0.05) (C) *becn1 cKO* mice increasingly used the looping search strategy and decreasingly used the spatial and sequential search strategy compared control mice after TBI, indicative of impairments in spatial learning and memory. Search strategy was analyzed using chi-squared analysis. (D) Novel object recognition (NOR) test was performed on days 16 and 17 following TBI to assess non-spatial memory retention in control and *becn1 cKO* mice. Quantification shows decrease in the ratio of time spent with the novel object as compared to familiar object in *becn1 cKO* mice after TBI, indicative of defects in non-spatial memory; n = 12 control sham, 13 *becn1 cKO* sham, 16 control TBI, and 14 *becn1 cKO* TBI mice. (E) Representative images of cresyl violet stained neurons in the dentate gyrus (DG) of the ipsilateral hippocampus (20X magnification) across all experimental groups. (F) Stereological quantification of data from (E) showed increased neuronal loss in the ipsilateral DG of *becn1 cKO* mice compared to control mice at 28 days post injury; n = 7–8 mice/group. (G) qRT-PCR based heatmap of innate immunity genes in sham and TBI (28 days post injury) control and *becn1 cKO* mice cortices. Color coding was based on z-score scaling; n = 4–5 mice/group. (H) MWM test demonstrating significantly improved spatial learning in wild-type mice treated with rapamycin following TBI; n = 12–14 mice/group. (I) qRT-PCR based heatmap of innate immunity genes at sham and 3 days post TBI in vehicle and rapamycin-treated mice cortices. Color coding was based on z-score scaling; n = 5–7 mice/group. (J) Western blot of cortical tissue lysates at 3 days post TBI demonstrated decreased inflammation in mice treated with rapamycin compared to vehicle-treated mice. All lanes are from the same western blot. (K) Densitometric quantification from (J) shows decreased protein levels of NLRP3, CGAS and STING1 in cortical tissue lysates at 3 days post injury in mice treated with rapamycin compared to vehicle treated mice; n = 4–5 mice/group. Data are mean ± SEM. ^0 < 0.05, ^^p < 0.01, ^^^^p < 0.0001 vs. corresponding sham, *p < 0.05 vs corresponding vehicle-treated mice; two-way ANOVA with Tukey's post-hoc for multiple comparisons.

Atg5 [49]. This suggests that similar autophagy-dependent mechanisms may contribute to both acute injury-induced, and age-related inflammatory changes observed in neurodegenerative diseases, and implicates inhibition of autophagy as one of the potential mechanisms contributing to increased rate of neurodegenerative diseases observed in people previously exposed to TBI.

Our data from WT mice demonstrate that following TBI, autophagy is inhibited in both activated microglia and infiltrating monocytes, suggesting the need to explore its function in both lineages. The *Lyz2-Cre* mice have been widely used to drive cre-mediated recombination in the myeloid cell lineage (monocytes, mature macrophages, and granulocytes) for the study of the peripheral innate immune response [50].

However, the efficiency of *Lyz2-cre* mediated recombination in microglia is less well-characterized. In the present study, we used cre-dependent *ROSA-tdTomato* reporter mice to demonstrate that *Lyz2-cre* is expressed in approximately 50% of the total microglial cells. Additionally, our NanoString and qRT-PCR analyses confirmed decrease in *Becn1* gene expression in the cortex of *Lyz2-cre Becn1-flox* mice with and without injury. Thus, *Lyz2-cre* is a suitable driver for gene knockout in microglia. Its use may be particularly advantageous for studies requiring simultaneous cre-mediated gene manipulation in both microglia and myeloid cells/monocytes. This is the case in TBI, where both microglia and infiltrating myeloid cells are known to contribute to neuroinflammation. Using the *becn1 cKO* (*Lyz2-cre Becn1-flox*) mice we were able to demonstrate that autophagy in microglia and infiltrating monocytes is necessary for prevention of excessive inflammatory responses following brain injury. Further studies using microglia and/or myeloid-specific cre drivers will be necessary to decipher the specific role and the relative contribution of autophagy in each lineage [8].

Studies of the peripheral immune responses suggest several mechanisms how autophagy may affect innate immune responses. They include removal of both extracellular and intracellular DAMPs as well as direct targeting of the components of innate immunity pathways by precision autophagy. Our work implicates inhibition of precision autophagy as a contributing factor to excessive neuroinflammation following TBI. Precision autophagy involves coordination between target recognition and assembly of the autophagic apparatus. In their autophagy roles, TRIM proteins act both as cargo receptors and as platforms for the assembly of the core autophagy regulators, such as ULK1 and BECN1 [27]. Our data demonstrate that similar to other autophagy receptors such as SQSTM1, levels of MEFV protein but not its mRNA increase after TBI, indicating inhibition in its degradation. ULK1-MEFV-NLRP3 complexes also accumulate after TBI, suggesting that precision autophagy targeting the NLRP3 inflammasome is activated but fails to proceed to completion after injury. This is consistent with the observed exacerbation of inflammasome activity. Since our data indicate that overall autophagy levels are decreased in microglia and infiltrating monocytes after injury, we expect that other precision autophagy pathways are similarly affected, contributing to overactivation of innate immunity pathways and overall increased inflammation. Direct involvement of autophagy in controlling levels of innate immunity mediators is also supported by the fact that their protein levels were decreased more than their mRNA following induction of autophagy by rapamycin treatment. Future work will be needed to further define the role of specific TRIM proteins and respective contributions of bulk and precision autophagy to regulation of innate immune responses after injury.

TBI-induced tissue damage causes accumulation of DAMP in the extracellular space. DAMP have been reported to play a crucial role in the pathogenesis of human autoimmune diseases [51] and their clearance is necessary to prevent prolonged inflammation in response to tissue injury, including in the context of TBI [52]. Levels of DAMP present after injury reflect both the extent of tissue damage and cell death and the efficiency of phagocytic clearance. Our work suggests that inhibition of autophagy causes defects in microglial phagocytosis which contribute to accumulation of DAMP within the injured cortex. Additionally, as we also observe increased neuronal cell loss in the hippocampal DG area of injured *Becn1 cKO* as compared to injured control mice, higher levels of neuroinflammation-induced neuronal cell death may also contribute to the observed DAMP accumulation.

In addition to canonical autophagy, a non-canonical autophagy pathway termed LC3-associated phagocytosis has been identified in professional phagocytes including macrophages [53]. LAP relies on many but not all the components of canonical autophagy and plays a role in clearance of extracellular pathogens, dead and dying cells and DAMP. While the role of LAP in prevention of autoimmune diseases has been characterized, much less is known about its function in the CNS. Our data indicate that like other forms of autophagy, LAP may be initiated in microglia and infiltrating myeloid cells after injury but fails to progress to completion. We expect that inhibition of LAP may also contribute to the observed accumulation of DAMP, excessive activation of innate immune pathways and increased inflammation after injury.

Our data indicate that TBI leads to inhibition of autophagy in activated microglia and infiltrating myeloid cells. Although the mechanisms leading to this inhibition remain unclear, our results suggest several potential contributing factors. As macrophages within the systemic circulation were not affected and inhibition of autophagy was restricted to microglia and infiltrating myeloid cells in the perilesional area, direct interaction with the highly pro-inflammatory environment likely plays a role [54]. However, as LPS treatment *in vitro* did not result in inhibition of flux, inflammatory stimulation *per se* appears to be insufficient and other factors may be involved. Potential contributors include reactive oxygen species (ROS) known to accumulate after injury and reported to both positively and negatively regulate cellular autophagy [55]. Additionally, oxidated lipid species abundant at the lesion site could play a role as has been reported in atherosclerosis models [56].

While neuroinflammation is an important contributor to neurotrauma damage, TBI pathology is complex and includes other components such as neurodegeneration and demyelination [7]. Therefore, development of an effective treatment will require addressing multiple pathological components. Our present data demonstrate that inhibition of autophagy in activated microglia and infiltrating macrophages after TBI drives increased inflammation and in particular activation of the innate immunity pathways, including the inflammasome and the type I IFN signaling. Both pathways have been previously shown to contribute to TBI neuropathology [57] and several studies demonstrated that their suppression or attenuation could improve functional outcomes after injury, confirming their functional importance [58]. Consistently, in our studies excessive activation of innate immune responses in *becn1 cKO* mice was associated with increased neuronal loss and worse cognitive outcomes after injury. Our previous work demonstrated that

autophagy is also inhibited in neurons after TBI, and that this inhibition contributes to neuronal cell death [29,30]. We also observed inhibition of autophagy in oligodendrocytes and others implicated it in oligodendrocyte differentiation [59]. Finally, our current data demonstrate improvement in functional recovery and decreased neuroinflammation in TBI mice treated with a well characterized autophagy activator, rapamycin. This is consistent with studies in other injury models where activation of autophagy could attenuate inflammation [60–63]. Therefore, reactivation or increasing autophagy presents a promising intervention avenue to address multiple TBI pathologies in several cell types, underscoring the need for better understanding of its mechanisms and function.

Materials and methods

Animals

All experiments were performed according to NIH guidelines for the care and use of animals in research and under protocol approved by IACUC at the University of Maryland, Baltimore. All experiments were performed on young adult male mice (9–12 weeks old, 21–27 g). Sham and CCI surgeries were performed on the following mice: *Cx3cr1*-GFP mice (The Jackson Laboratory, 005582), *Ccr2*-RFP mice (The Jackson Laboratory, 017586), *C57Bl/6* mice (The Jackson Laboratory, 00064), transgenic *C57Bl/6* mice expressing GFP-LC3 [64], ROSA^{tdTomato} mice (The Jackson Laboratory, 007914), *Lyz2/LyzM-Cre* mice (The Jackson Laboratory, 004781) and *Becn1/Beclin*$^{flox/flox}$ mice (The Jackson Laboratory, 028794). *Lyz2/LyzM-Cre* mice and *Becn1/Beclin*$^{flox/flox}$ mice were crossed with each other for two generations to produce *Becn1*$^{flox/flox}$; *Lyz2*$^{Cre/Cre}$ knockout mice, all mice genotyped for flox and Cre alleles according to the The Jackson Laboratory genotyping protocol. All mice were housed on sterilized bedding in a specific pathogen- free facility (12 h light/dark cycle).

Controlled cortical impact (CCI)

TBI was performed on mice using a custom-designed controlled cortical impact (CCI) injury device consisting of a microprocessor- controlled pneumatic impactor as described previously [29,30]. After mice were anesthetized with an inducing concentration of 3% isoflurane, a 10 mm midline incision was made over the skull. The skin and fascia were retracted, and a 4 mm craniotomy was made on the central aspect of the left parietal bone. Moderate TBI was induced by the microprocessor-controlled and compressed air driven pneumatic impactor of 3.5 mm diameter tip with the impact velocity of 6 m/s and a deformation depth of 2 mm. In sham animals, the same procedure was performed except for the craniotomy and impact.

Cell lines

Murine RAW 246.7 macrophages (ATCC, TIB-71) and murine IMG microglial cells (a generous gift of Shankar Chinta, Buck Institute, who obtained them from the original source) [65] and were cultured in cell culture media containing DMEM (Gibco, 11,995,065), 10% heat-inactivated fetal bovine serum (FBS, Sigma-Aldrich, N4762) and 1% penicillin-streptomycin (Thermo Fisher Scientific, 15,240,062).

BMDM isolation and culture

BMDMs were isolated from the marrow of the femurs and tibias of *Becn1*$^{flox/flox}$*Lyz2*$^{Cre/Cre}$ *(becn1 cKO), Lyz2*$^{Cre/Cre}$, and *C57Bl/6* mice following euthanasia and processed as previously described [66]. Briefly, the marrow was flushed out into a sterile falcon tube in DMEM supplemented with heat-inactivated 10% FBS and 1% penicillin-streptomycin to obtain a single cell suspension. The cell suspension was triturated using a sterile Pasteur pipette, filtered through a 70-μm nylon mesh filter into a sterile tube and centrifuged (400 × *g*, 5 min). The supernatant was removed, and the remaining pellet was DMEM supplemented with 20% L929-conditioned media [66].

Cells were seeded in sterile cell culture flasks (T-175 cm^2 flasks). On day 2, non-adherent cells were removed from the flask, the media was replaced, and the remaining adherent cells were maintained in culture for a further 6 days, with media being replaced on day 4. On day 6, cells were transferred to 6-well plates (0.5×10^6 cells per well) and cultured for another 2 days, after which time they were scraped off and processed for downstream analysis or plated for in vitro experiments.

In vitro drug treatments

24 h prior to *in vitro* experiment, cells were passaged and plated in 24-well plates at a density of 5×10^4 cells per well. Specified cells were pre-treated with LPS (10 ng/ml; Sigma, L2630), 3 h prior to drug treatment. The following autophagy inhibitors were used: Bafilomycin A_1 (BafA) (20 nM; Sigma-Aldrich, B1793), 3-MA (100 μM; Sigma-Aldrich, M9281) and MRT68921 (10 μM; Sigma-Aldrich, SML1644). Treatment with the inhibitors was carried out for 6 h, following which all samples were lysed in Laemmli buffer and processed for western blotting. For all *in vitro* experiments, n = 3 replicates/group with 3 independent experiments performed.

Rapamycin treatment

Rapamycin (Sigma, 37,094) was dissolved in DMSO and then diluted in vehicle containing 0.25% PEG400 (Sigma, 202,398) and 0.25% Tween 80 (Sigma, P4780), as previously described [29]. The final concentration of DMSO in the vehicle was adjusted to 0.1%. Rapamycin was injected intra-peritoneally in *C57Bl/6* mice at a dose of 5 mg/kg, starting at 30 min post TBI, and then once each day. Mice processed for western blot and qRT-PCR were treated with rapamycin up to day 3 post TBI; mice used for behavioral assessment were treated up to day 7 post TBI. Control mice were injected with the vehicle only.

Western blot

For *in vivo* samples, experimental mice were anesthetized, perfused with ice-cold saline, and decapitated. Approximately 75 mg of cortical brain was isolated from sham and TBI mice (for TBI samples, this cortical tissue collected was approximately 5 mm of the cortical area surrounding the ipsilateral injury site) and homogenized in RIPA buffer (TekNova, R3792) with protease inhibitor (Roche, 11,836,170,001) and phosphatase inhibitors (Sigma, P5792) as described previously [67]. Cell lysates were prepared by lysing the IMG cells, RAW 246.7 cells and BMDM cultured in cell culture plates with SDS-PAGE buffer. All lysates were resolved on 4–20% SDS-PAGE gels (Bio-Rad Laboratories, 5,671,095) and transferred to PVDF membrane (Millipore Sigma, IPVH00010) using semi-dry transfer. Membranes were blocked with 5% nonfat milk, probed with primary antibodies overnight at 4°C and incubated with HRP-conjugated secondary antibodies (Sera-Care KPL, 474–1506, 474–1806, 14–16–06 and 14–13–06) in blocking solution at room temperature for 1 h. Protein bands were detected using SuperSignal West Dura Extended Duration Substrate (Thermo Fisher Scientific, 34,076), SuperSignal Femto Chemiluminescent Substrate (Thermo Fisher Scientific, 34,080) or SuperSignal West Pico Chemiluminescent Substrate (Thermo Fisher Scientific, 34,080) and visualized using Chemi-doc system (Bio-Rad Laboratories, Universal Hood II). Band intensity was analyzed using Image Lab software (Bio-Rad Laboratories) and normalized to loading control.

The following primary antibodies were used:

CYBB/NOX2 (1:1000; BD Biosciences, 611,415), CGAS (1:1000; Cell Signaling Technology, 15,102), STING1 (1:1000; Cell Signaling Technology, 13,647), LC3 (1:1000; Novus, NB100–2220), SQSTM1/p62 (1:1000; BD Biosciences, 610,833), NOS2/iNOS (1:1000; BD Biosciences, 610,328), NLRP3 (1:1000; Cell Signaling Technology, 15,101), BECN1 (1:1000; Santa Cruz Biotechnology, sc-11,427), ACTB/β-Actin (1:10,000; Sigma, A1978), MEFV/TRIM20 (1:1000; Proteintech, 24,280-1-AP), SPTAN1/α-FODRIN (1:10,000; Enzo Life Sciences, BML-FG6090).

Nitric oxide assay

NO production was assayed using the Griess Reagent Assay (Invitrogen, G7921), according to the manufacturer's instructions.

Immunohistochemistry

Experimental mice were anesthetized with isoflurane, and transcardially perfused with cold saline and then with 4% paraformaldehyde (PFA, pH 7.4). Brains were removed and post-fixed in PFA for 24 h and then protected in 30% sucrose. Mice brains were cut into 20 µm frozen sections on glass slides as described previously [29,30]. Sections were blocked with 5% goat serum (Millipore, S30-100) in 1X phosphate-buffered saline (PBS; Quality Biological, INC., 119–069-101) containing 0.025% Triton X-100 (Sigma, T8787). Sections were incubated overnight with primary antibodies at 4°C and then with secondary antibodies in the blocking solution for 2 h at room temperature. Nuclei were stained with 1 µg/ml DAPI (Sigma-Aldrich,10,236,276,001), and mounted with glass coverslips using Hydromount solution (National Diagnostics, 50–899-90,144).

Primary antibodies used include: CYBB/NOX2 (1:1000; BD Biosciences, 611,414), NLRP3 (1:200; Cell Signaling Technology, 15,101), NOS2/iNOS (1:250; BD Biosciences), AIF1/IBA1 (1:1000; Wako, 019–19,741), SQSTM1/p62 (1:200; Progen, GP62-C), ADGRE1/F4/80 (1:500; Thermo Fisher Scientific, MA1-91,124), and TMEM119 (1:200, Cell Signaling Technology, 90,840). Secondary antibodies include: Alexa Fluor 488 goat anti-rabbit (Invitrogen, A-11034), Alexa Fluor 546 goat anti-rabbit (Invitrogen, A-11035), Alexa Fluor 546 goat anti-mouse (Invitrogen, A-11030), Alexa Fluor 546 goat anti-rat (Invitrogen, A-11081), Alexa Fluor 633 goat anti-Guinea pig (Invitrogen, A-11075).

Images were acquired using a fluorescence Nikon Eclipse Ti-E/Ni-E microscope and analyzed and quantified by Elements software (V4.12.01, Nikon). Emission wavelengths included 460 nm (DAPI), 535 nm (GFP-LC3, CX3CR1-GFP, and Alexa Fluor 488), 620 nm (Alexa Fluor 546) and 670 nm (Alexa Fluor 633). Exposure times were kept constant for all sections in each experiment. GPL-LC3 images and other images quantification. Quantification was performed using Elements software as described: nuclei were identified using Spot Detection algorithm; cells positive for IF markers were identified using Detect Regional Maxima algorithm, followed by global thresholding [30]. Number of positive cells was normalized to the total number of cells imaged.

Flow cytometry

Experimental mice were anesthetized with isoflurane, and transcardially perfused with cold saline. Cortical tissue from sham and injured mice were removed and processed by mechanical disruption on a 70 µm filter screen and resuspended in RPMI-1640 (Quality Biological, 112–025-101). Ten Units (U) papain (Sigma-Aldrich, P4762), 10 mg/ml DNase II (Sigma, 10,104,159,001), 1 mg/ml collagenase-dispase (Sigma, 10,269,638,001), and 1 µl of GolgiPlug containing brefeldin A (BD Biosciences, 555,029) were added to the brain suspension and incubated on a shaker at 200 rotations per minute for 1 h at 37°C for mechanical and enzymatic digestion of the brain tissue. After incubation, leukocytes were separated from other brain cells by a Percoll gradient (GE Healthcare, GE17-5445-02). Brain leukocytes were resuspended in 70% Percoll-HBSS and were slowly injected under a 30% Percoll-RPMI layer using a pipetting needle with blunt end (Sigma, CAD7942). This Percoll gradient was centrifuged for 20 min at 400 × *g*, with no brake. The myelin layer was removed from the top of the 30% Percoll layer and leukocytes were then retrieved from the interface of the 30% and 70% Percoll layers and resuspended in RPMI as single cell suspensions. These leukocytes were then washed in fluorescence-activated cell sorter (FACS) buffer (5% FBS and 0.1% penicillin and streptomycin in 1xHBSS) with sodium azide and blocked with 1:50 mouse Fc Block (clone 93; eBioscience, 14–0161-82) for

10 min on ice prior to staining with primary antibody-conjugated fluorophores. After primary antibody staining, cells were washed in Fixation/Permeabilization solution (BD Biosciences, 554,722) for 20 minutes and washed twice in Permeabilization/Wash Buffer (BD Biosciences, 554,723) and resuspended in an intracellular antibody cocktail of cytokine antibodies. After intracellular antibody staining for 30 min at 4°C, samples were washed with Wash Buffer, fixed with 2% PFA and finally resuspended in PBS (Corning, 21–040). Samples are stored at 4°C until they are to be used for analysis in the flow cytometer.

To assess phagocytic ability, TexasRed fluorescent carboxylate-modified polystyrene latex beads (0.5-µm mean diameter; Sigma, L3030) were added to freshly isolated cells in a final dilution of 1:500 (in RPMI) stained for surface markers and viability and fixed in 2% PFA and resuspended in FACS buffer to be analyzed on the flow cytometer.

Surface staining included: from PTPRC/CD45-eF450 (Thermo Fisher, 48–0451-82), ITGAM/CD11B-APCeF780 (Thermo Fisher, 47–0112-82), LY6C-AF700 (Biolegend, 128,023) and LY6G-APC (Thermo Fisher, 17–9668-82) at final concentration of 1:100 for each antibody. To mark autophagy flux levels, Cyto-ID® Autophagy Detection Kit (Enzo Life Sciences, ENZ-51031-0050) was added at a dilution of 1:1000, as per the manufacturer's instructions. For live/dead cell discrimination, a fixable viability dye, Zombie Aqua™ (Biolegend, 423,101), was dissolved in DMSO according to the manufacturer's instructions and added to cells at a final concentration of 1:50. Intracellular antibodies included TNF-PE-Cy7 (1:50, Biolegend, 502,929), IL1B/IL-1β-PerCP-eF710 (1:100, NJTEN3, Invitrogen, 46–7114-82), LC3B-FITC (1:100, Novus Biologicals, NB100-2220 F) and SQSTM1/p62-AF647 (1:50, Novus Biologicals, 2821AF647).

Data were acquired on a BD LSRII flow cytometer equipped with FACsDiva 6.0 (BD Biosciences, San Jose, CA) and analyzed using FCS Express™ 7 (De Novo Software, Glendale, CA).

qRT-PCR

Total RNA isolated from BMDM and ipsilateral cortex of sham and injured mice using Trizol reagent (Invitrogen, 15,596–018) was converted into cDNA using the Verso cDNA Synthesis Kit (Thermo Scientific, AB1453B) as per the manufacturer's instruction. cDNA TaqMan Universal Master Mix II (Applied Biosystems, 4,440,040) was used to perform quantitative real-time PCR amplification. Briefly, reactions were performed in duplicate by mixing 2X TaqMan Universal Master Mix II, 1 ml of cDNA (corresponding to 50 ng RNA/reaction) and 20 µl TaqMan Gene Expression Assay, in a final volume of 20 ml.

TaqMan Gene Expression assays for the following genes were used for mouse:

Gapdh (Mm99999915_g1), *Nlrp3* (Mm00840904_m1), *Cybb* (Mm01287743_m1), *Cgas* (Mm01147496_m1), *Sting1* (Mm01158117_m1), *Il1b* (Mm00434228_m1), *Casp1* (Mm01275139_m1), *Trim20/Mefv* (Mm00490258_m1), *Lcn2* (Mm01324470_m1), *Nfkb1* (Mm00476361_m1, *Becn1* (Mm01265461_m1), *Il10* (Mm01288386_m1), *Ifnb1* (Mm00439552_s1).

Reactions were amplified and quantified by using a 7900HT Fast Real-Time PCR System and the corresponding software (Applied Biosystems). The PCR profile consisted of 1 cycle at 50°C for 2 minutes and 95°C for 10 min, followed by 40 cycles at 95°C for 15s and 60°C for 1 min. Gene expression was normalized to *Gapdh*, and the relative quantity of mRNAs was calculated based on the comparative Ct method.

NanoString analysis

Experimental mice were anesthetized with isoflurane, perfused with ice-cold saline, and decapitated. Approximately 75 mg of cortical brain was isolated from sham and TBI mice (for TBI samples, the cortical tissue collected was approximately 5 mm of the cortical area surrounding the ipsilateral injury site). RNA was from isolated using Trizol reagent (Invitrogen, 15,596–018). Total RNA (20 ng/µl) was run on a NanoString nCounter® system for Mouse Neuroinflammation v1.0 panel (NanoString Technologies, Seattle, WA) to profile RNA transcript counts for 757 genes and 13 housekeeping genes. Sample gene transcript counts were normalized prior to downstream analysis and pairwise differential expression analysis was performed with NanoString's nSolver software Version 4.0. Partial Least Square Discriminant analysis (PL-SDA) and overall heatmap were generated using MetaboAnalyst 3.0. Subsets of genes displayed as heatmaps were normalized across samples as z-scores and then averaged to a single value per group before plotting with GraphPad Prism. Pathway analyses, including Gene Functional Classification and Functional Annotation Clustering were performed using NIH DAVID Bioinformatics Resources [68].

Immunoprecipitation (IP)

Approximately 75 mg of ipsilateral cortical brain was isolated from sham and injured mice were homogenized in RIPA buffer. Protein concentration was calculated using bicinchoninic acid assay

(BCA; Thermo Fisher Scientific, 23,225). Equal quantities of protein were pre-cleared with Pierce Protein A/G/Agarose Beads (Thermo Fisher Scientific, 20,421) for 1 h and incubated with primary antibody rotating overnight at 4°C. On the following day, agarose beads were added and incubated for 1–2 h rotating at 4°C. Beads were washed 4 times and samples were eluted in Laemmli sample buffer followed by western blot analysis. The following antibodies were used for the IP: ULK1 (1:100; Cell Signaling Technology, 8054), Rabbit IgG (1:100; Cell Signaling Technology, 2729)

Neurobehavioral tests

Beam Walk: Fine motor coordination was assessed using the beam walk test as previously described [43]. Briefly, mice were placed at the end of a wooden beam (5 mm wide, 120 mm long) and the number of slips (foot faults) of the right hind limb were recorded over 50 steps. Mice were trained on the

beam walk for 3 days prior to surgery and tested at 1-, 3-, 7-, 14-, 21-, and 28 days after TBI. Gross motor function was also assessed during the habituation stage of novel object recognition testing (distance travel) and during Morris Water Maze testing (average swim speed) using Any-Maze software (Stoelting Company, Wood Dale, IL).

Novel Object Recognition (NOR): Non-spatial memory in mice was assessed by performing NOR testing through 15–17 days after TBI as previously described [69]. On test day, mice were allowed to freely explore for until 20 seconds of total interaction between the objects was recorded. Novel/familiar objects and the side in which the novel object was positioned were balanced across all experimental groups to control for any potential object and side biases. Testing was recorded using Any-Maze software. Novel object preference was quantified as the ratio of time spent with the novel object to the time spent with the familiar object.

Morris Water Maze (MWM): Hippocampal- dependent spatial learning and memory were assessed using the MWM during 21–25 days after TBI as previously described [62]. A circular tank (100 cm in diameter) was filled with water (24 ± 2°C) and was surrounded by various extra-maze on the inner walls of the testing area. A transparent platform (10 cm in diameter) was submerged 0.5 cm below the surface of the water. Mice were trained to find the hidden submerged platform located in the northeast (NE) quadrant of the tank for 4 consecutive days. The mice underwent four trials per day, starting from a randomly selected release point (east, south, west, and north). Each mouse was allowed a maximum of 90s to find the hidden submerged platform. Reference memory was assessed by a probe test performed 24 h after the final acquisition day, wherein the platform was removed, and the mice were released from the southwest position, and the time in the target quadrant was recorded. Testing was recorded using Any-Maze software.

Search strategy analysis was performed, characterized as follows: 1). Spatial search strategy: swimming directly to platform with no more than one loop or swimming directly to the correct target quadrant and searching for the platform; 2). Sequential search strategy: searching the interior portion of or the entire tank without spatial bias, including searching within the incorrect target quadrant before finding platform; and 3). Looping search strategy: circular swimming around the tank, swimming in tight circles, or swimming around the wall of the tank before finding the submerged hidden platform.

Y-maze spontaneous alternation: The Y-maze behavior test, to assess hippocampal-dependent working (short-term) memory, was performed on day 8 post TBI as described previously [70]. The Y-maze apparatus (Stoelting Co.) consisted of three identical arms, each arm 35-cm long, 5-cm wide, and 10 cm high, at an angle of 120° with respect to the other arms. One arm was selected as the starting arm, and the mouse was placed within and allowed to explore the maze freely for 6 minutes. Arm entries (arms A-C) were recorded by analyzing mouse activity using Any-Maze tracking software. An arm entry was attributed when all four paws of the mouse entered the arm, and an alternation was determined when the mouse entered three different arms consecutively. The percentage of alternation was calculated as follows: [Total number of alternations/(total arm entries −2)] * 100.

Histology

Lesion Volume: Cortical lesion volume was assessed mouse brain cortical sections at 28 days after TBI. Sixty-µm fixed brain sections located approximately 240 cm apart across the entire lesion volume were stained with cresyl violet (FD Neurotechnologies Inc., NC0527137) and images were acquired on Leica DM4000 B TL (BF) microscope. Quantification was based on the Cavalieri method using StereoInvestigator software (MBF Biosciences) and the lesion volume was quantified by outlining the missing tissue on the injured hemisphere using the Cavalieri estimator with a grid spacing of 0.1 mm.

Hippocampal Neuronal Count: Analysis of neuronal cell loss in ipsilateral hippocampus was performed on 60-µm fixed mouse brain cortical sections stained with cresyl violet, collected at 28 days after TBI. A total of 5 sections per brain (every fourth 60-µm section between −1.34 and −2.54 mm and −2.7 to −3.16 mm from bregma) were analyzed. Neuronal cell loss was quantified using a Leica DM4000B microscope (Leica Microsystems) with the StereoInvestigator software (MBF Biosciences) by counting the number of cresyl violet stained neurons representing surviving neurons using the optical fractionator method of unbiased stereology, with fewer cresyl violet stained neurons representing decreased neuronal counts. The volume of the regions counted was determined using the Cavalieri method. Results are expressed in terms of cellular density (cells/mm^3).

Statistical analyses

Quantitative data were expressed as mean ± standard error of the mean (SEM) and statistical analysis was performed using GraphPad Prism Software v. 9.2 (GraphPad Software, Inc., La Jolla, CA), and a $p < 0.05$ was chosen as minimal value for statistical significance. Immunofluorescence (IF) quantification was analyzed using one-way AVOVA with Dunnett's post-hoc. Beam walk data was acquired by repeated measures two-way ANOVA to determine the interactions of time and injury and genotype changes, followed by post-hoc adjustments using a Tukey's multiple comparison test. Gene expression levels by qRT-PCR and NanoString, protein expression levels by western blotting, flow cytometry data and behavioral outcomes (average distance traveled, novel object preference, time spent in the escape quadrant, average swim speeds) were analyzed by two-way ANOVA, followed by post-hoc adjustments using a Tukey's or Bonferroni post-hoc for multiple comparisons. The MWM search strategy was analyzed using a chi-square analysis. For immunohistochemistry, neuronal cell counts were analyzed by two-way ANOVA, followed by Tukey's post-hoc, and lesion volume was analyzed using unpaired, two-tailed Student t-test. Statistical tests for each experiment are included in figure legends.

Acknowledgments

We would like to thank Ms. Courtney Merryman for technical assistance with histology, Ms. Yulemni Morel for assistance with data analysis, and Dr. Xiaoxuan Fan for technical assistance with flow cytometry.

Disclosure statement

No potential conflict of interest was reported by the authors.

Funding

This work was supported by the NIH [R01NS094527]; NIH [R01NS091218, R01NS115876].

ORCID

Marta M. Lipinski http://orcid.org/0000-0002-7537-9014

References

[1] Acosta SA, Tajiri N, Shinozuka K, et al. Combination therapy of human umbilical cord blood cells and granulocyte colony stimulating factor reduces histopathological and motor impairments in an experimental model of chronic traumatic brain injury. PLoS One. 2014;9(3):e90953.
[2] Maas AI, Stocchetti N, Bullock R. Moderate and severe traumatic brain injury in adults. Lancet Neurol. 2008 Aug;7(8):728–741.
[3] Bryant RA, O'Donnell ML, Creamer M, et al. The psychiatric sequelae of traumatic injury. Am J Psychiatry. 2010 Mar;167(3):312–320.
[4] Li Y, Li Y, Li X, et al. Head injury as a risk factor for dementia and Alzheimer's disease: a systematic review and meta-analysis of 32 observational studies. PLoS One. 2017;12(1):e0169650.
[5] Shively S, Scher AI, Perl DP, et al. Dementia resulting from traumatic brain injury: what is the pathology? Arch Neurol. 2012 Oct;69(10):1245–1251.
[6] Faden AI, Stoica B. Neuroprotection: challenges and opportunities. Arch Neurol. 2007 Jun;64(6):794–800.
[7] Loane DJ, Faden AI. Neuroprotection for traumatic brain injury: translational challenges and emerging therapeutic strategies. Trends Pharmacol Sci. 2010 Dec;31(12):596–604.
[8] Morganti JM, Jopson TD, Liu S, et al. CCR2 antagonism alters brain macrophage polarization and ameliorates cognitive dysfunction induced by traumatic brain injury. J Neurosci. 2015 Jan 14;35(2):748–760.
[9] Henry RJ, Ritzel RM, Barrett JP, et al. Microglial depletion with CSF1R inhibitor during chronic phase of experimental traumatic brain injury reduces neurodegeneration and neurological deficits. J Neurosci. 2020 Apr 1;40(14):2960–2974.
[10] Russo MV, McGavern DB. Inflammatory neuroprotection following traumatic brain injury. Science. 2016 Aug 19;353(6301):783–785.
[11] Block ML, Zecca L, Hong JS. Microglia-mediated neurotoxicity: uncovering the molecular mechanisms. Nat Rev Neurosci. 2007 Jan;8(1):57–69.
[12] Ramlackhansingh AF, Brooks DJ, Greenwood RJ, et al. Inflammation after trauma: microglial activation and traumatic brain injury. Ann Neurol. 2011 Sep;70(3):374–383.
[13] Loane DJ, Kumar A. Microglia in the TBI brain: the good, the bad, and the dysregulated. Exp Neurol. 2016 Jan;275(Pt 3):316–327.
[14] Morganti JM, Riparip LK, Rosi S. Call off the dog(ma): M1/M2 polarization is concurrent following traumatic brain injury. PLoS One. 2016;11(1):e0148001.
[15] Begemann M, Leon M, van der Horn HJ, et al. Drugs with anti-inflammatory effects to improve outcome of traumatic brain injury: a meta-analysis. Sci Rep. 2020 Sep 30;10(1):16179.
[16] Mizushima N, Levine B, Cuervo AM, et al. Autophagy fights disease through cellular self-digestion. Nature. 2008 Feb 28;451(7182):1069–1075.
[17] Shao BZ, Yao Y, Zhai JS, et al. The role of autophagy in inflammatory bowel disease. Front Physiol. 2021;12:621132.
[18] Wang Y, Li YB, Yin JJ, et al. Autophagy regulates inflammation following oxidative injury in diabetes. Autophagy. 2013 Mar;9(3):272–277.
[19] Yang Z, Goronzy JJ, Weyand CM. Autophagy in autoimmune disease. J Mol Med (Berl). 2015 Jul;93(7):707–717.
[20] Wu J, Lipinski MM. Autophagy in neurotrauma: good, bad, or dysregulated. Cells. 2019 Jul 10;8(7):693.
[21] Deretic V, Levine B. Autophagy balances inflammation in innate immunity. Autophagy. 2018;14(2):243–251.
[22] Martinez J, Malireddi RK, Lu Q, et al. Molecular characterization of LC3-associated phagocytosis reveals distinct roles for Rubicon, NOX2 and autophagy proteins. Nat Cell Biol. 2015 Jul;17(7):893–906.
[23] Boada-Romero E, Martinez J, Heckmann BL, et al. The clearance of dead cells by efferocytosis. Nat Rev Mol Cell Biol. 2020 Jul;21(7):398–414.
[24] Sil P, Muse G, Martinez J. A ravenous defense: canonical and non-canonical autophagy in immunity. Curr Opin Immunol. 2018 Feb;50:21–31.
[25] Deretic V. Autophagy in inflammation, infection, and immunometabolism. Immunity. 2021 Mar 9;54(3):437–453.
[26] Deretic V, Saitoh T, Akira S. Autophagy in infection, inflammation and immunity. Nat Rev Immunol. 2013 Oct;13(10):722–737.
[27] Kimura T, Jain A, Choi SW, et al. TRIM-mediated precision autophagy targets cytoplasmic regulators of innate immunity. J Cell Biol. 2015 Sep 14;210(6):973–989.
[28] Mandell MA, Jain A, Arko-Mensah J, et al. TRIM proteins regulate autophagy and can target autophagic substrates by direct recognition. Dev Cell. 2014 Aug 25;30(4):394–409.
[29] Sarkar C, Zhao Z, Aungst S, et al. Impaired autophagy flux is associated with neuronal cell death after traumatic brain injury. Autophagy. 2014;10(12):2208–2222.
[30] Sarkar C, Jones JW, Hegdekar N, et al. PLA2G4A/cPLA2-mediated lysosomal membrane damage leads to inhibition of autophagy and neurodegeneration after brain trauma. Autophagy. 2020 Mar;16(3):466–485.
[31] Kumar A, Alvarez-Croda DM, Stoica BA, et al. Microglial/macrophage polarization dynamics following traumatic brain injury. J Neurotrauma. 2016 Oct 1;33(19):1732–1750.
[32] Yona S, Kim KW, Wolf Y, et al. Fate mapping reveals origins and dynamics of monocytes and tissue macrophages under homeostasis. Immunity. 2013 Jan 24;38(1):79–91.
[33] Ichimura Y, Kominami E, Tanaka K, et al. Selective turnover of p62/A170/SQSTM1 by autophagy. Autophagy. 2008 Nov;4(8):1063–1066.
[34] Klionsky DJ, Petroni G, Amaravadi RK, et al. Autophagy in major human diseases. EMBO J. 2021 Oct 1;40(19):e108863.
[35] Ritzel RM, Li Y, Lei Z, et al. Functional and transcriptional profiling of microglial activation during the chronic phase of TBI identifies an age-related driver of poor outcome in old mice. Geroscience. 2022 Jun;44(3):1407–1440.
[36] Thayer JA, Awad O, Hegdekar N, et al. The PARK10 gene USP24 is a negative regulator of autophagy and ULK1 protein stability. Autophagy. 2020 Jan;16(1):140–153.
[37] Clausen BE, Burkhardt C, Reith W, et al. Conditional gene targeting in macrophages and granulocytes using LysMcre mice. Transgenic Res. 1999 Aug;8(4):265–277.
[38] Madisen L, Zwingman TA, Sunkin SM, et al. A robust and high-throughput Cre reporting and characterization system for the whole mouse brain. Nat Neurosci. 2010 Jan;13(1):133–140.
[39] McKnight NC, Zhong Y, Wold MS, et al. Beclin 1 is required for neuron viability and regulates endosome pathways via the UVRAG-VPS34 complex. PLoS Genet. 2014 Oct;10(10):e1004626.
[40] Di Rienzo M, Romagnoli A, Antonioli M, et al. TRIM proteins in autophagy: selective sensors in cell damage and innate immune responses. Cell Death Differ. 2020 Mar;27(3):887–902.

[41] Shichita T, Ito M, Morita R, et al. MAFB prevents excess inflammation after ischemic stroke by accelerating clearance of damage signals through MSR1. Nat Med. 2017 Jun;23(6):723–732.
[42] Zhao Z, Loane DJ, Murray MG 2nd, et al. Comparing the predictive value of multiple cognitive, affective, and motor tasks after rodent traumatic brain injury. J Neurotrauma. 2012 Oct 10;29 (15):2475–2489.
[43] Kabadi SV, Stoica BA, Hanscom M, et al. CR8, a selective and potent CDK inhibitor, provides neuroprotection in experimental traumatic brain injury. Neurotherapeutics. 2012 Apr;9 (2):405–421.
[44] Saitoh T, Fujita N, Yoshimori T, et al. [Autophagy and innate immunity]. Tanpakushitsu Kakusan Koso. Protein, Nucleic Acid, Enzyme. 2008 Dec;53(16 Suppl):2279–2285.
[45] Saederup N, Cardona AE, Croft K, et al. Selective chemokine receptor usage by central nervous system myeloid cells in CCR2-red fluorescent protein knock-in mice. PLoS One. 2010 Oct 27;5(10):e13693.
[46] Lodder WL, Vogel WV, Lange CA, et al. Detection of extranodal spread in head and neck cancer with [18F]FDG PET and MRI: improved accuracy? Q J Nucl Med Mol Imaging. 2015 Sep;59 (3):327–335.
[47] Wei HL, Ma SQ, Li CX. Deficiency of unc-51 like kinase 1 (Ulk1) protects against mice traumatic brain injury (TBI) by suppression of p38 and JNK pathway. Biochem Biophys Res Commun. 2018 Sep 5;503(2):467–473.
[48] Chen Y, Meng J, Xu Q, et al. Rapamycin improves the neuroprotection effect of inhibition of NLRP3 inflammasome activation after TBI. Brain Res. 2019 May 1;1710:163–172.
[49] Cheng J, Liao Y, Dong Y, et al. Microglial autophagy defect causes Parkinson disease-like symptoms by accelerating inflammasome activation in mice. Autophagy. 2020 Dec;16(12):2193–2205.
[50] Shi J, Hua L, Harmer D, et al. Cre driver mice targeting macrophages. Methods Mol Biol. 2018;1784:263–275.
[51] Roh JS, Sohn DH. Damage-associated molecular patterns in inflammatory diseases. Immune Netw. 2018 Aug;18(4):e27.
[52] Braun M, Vaibhav K, Saad NM, et al. White matter damage after traumatic brain injury: a role for damage associated molecular patterns. Biochim Biophys Acta Mol Basis Dis. 2017 Oct;1863 (10Pt B):2614–2626.
[53] Martinez J, Almendinger J, Oberst A, et al. Microtubule-associated protein 1 light chain 3 alpha (LC3)-associated phagocytosis is required for the efficient clearance of dead cells. Proc Natl Acad Sci U S A. 2011 Oct 18;108(42):17396–17401.
[54] Levine B, Mizushima N, Virgin HW. Autophagy in immunity and inflammation. Nature. 2011 Jan 20;469(7330):323–335.
[55] Zhou J, Li XY, Liu YJ, et al. Full-coverage regulations of autophagy by ROS: from induction to maturation. Autophagy. 2022 Jun;18(6):1240–1255.
[56] Sheedy FJ, Grebe A, Rayner KJ, et al. CD36 coordinates NLRP3 inflammasome activation by facilitating intracellular nucleation of soluble ligands into particulate ligands in sterile inflammation. Nat Immunol. 2013 Aug;14(8):812–820.
[57] Xu X, Yin D, Ren H, et al. Selective NLRP3 inflammasome inhibitor reduces neuroinflammation and improves long-term neurological outcomes in a murine model of traumatic brain injury. Neurobiol Dis. 2018;117:15–27.
[58] Abdullah A, Zhang M, Frugier T, et al. STING-mediated type-I interferons contribute to the neuroinflammatory process and detrimental effects following traumatic brain injury. J Neuroinflammation. 2018 Nov 21;15(1):323.
[59] Smith CM, Mayer JA, Duncan ID. Autophagy promotes oligodendrocyte survival and function following dysmyelination in a long-lived myelin mutant. J Neurosci. 2013 May 1;33 (18):8088–8100.
[60] Ko JH, Yoon SO, Lee HJ, et al. Rapamycin regulates macrophage activation by inhibiting NLRP3 inflammasome-p38 MAPK-NFkappaB pathways in autophagy- and p62-dependent manners. Oncotarget. 2017 Jun 20;8(25):40817–40831.
[61] Carames B, Hasegawa A, Taniguchi N, et al. Autophagy activation by rapamycin reduces severity of experimental osteoarthritis. Ann Rheum Dis. 2012 Apr;71(4):575–581.
[62] Liu Z, Chen D, Chen X, et al. Trehalose induces autophagy against inflammation by activating TFEB signaling pathway in human corneal epithelial cells exposed to hyperosmotic stress. Invest Ophthalmol Vis Sci. 2020 Aug 3;61(10):26.
[63] Li Y, Lei Z, Ritzel RM, et al. Impairment of autophagy after spinal cord injury potentiates neuroinflammation and motor function deficit in mice. Theranostics. 2022;12(12):5364–5388.
[64] Mizushima N, Yamamoto A, Matsui M, et al. In vivo analysis of autophagy in response to nutrient starvation using transgenic mice expressing a fluorescent autophagosome marker. Mol Biol Cell. 2004 Mar;15(3):1101–1111.
[65] McCarthy RC, Lu DY, Alkhateeb A, et al. Characterization of a novel adult murine immortalized microglial cell line and its activation by amyloid-beta. J Neuroinflammation. 2016 Jan;27 (13):21.
[66] Barrett JP, Costello DA, O'Sullivan J, et al. Bone marrow-derived macrophages from aged rats are more responsive to inflammatory stimuli. J Neuroinflammation. 2015 Apr;9(12):67.
[67] Barrett JP, Henry RJ, Shirey KA, et al. Interferon-beta plays a detrimental role in experimental traumatic brain injury by enhancing neuroinflammation that drives chronic neurodegeneration. J Neurosci. 2020 Mar 11;40(11):2357–2370.
[68] Huang da W, BT S, RA L. Systematic and integrative analysis of large gene lists using DAVID bioinformatics resources. Nat Protoc. 2009;4(1):44–57.
[69] Hanscom M, Loane DJ, Aubretch T, et al. Acute colitis during chronic experimental traumatic brain injury in mice induces dysautonomia and persistent extraintestinal, systemic, and CNS inflammation with exacerbated neurological deficits. J Neuroinflammation. 2021 Jan 18;18(1):24.
[70] Kumar A, Barrett JP, Alvarez-Croda DM, et al. NOX2 drives M1-like microglial/macrophage activation and neurodegeneration following experimental traumatic brain injury. Brain Behav Immun. 2016;58:291–309.